

**Assessment of Marker-Controlled
Watershed segmentation
algorithm for individual tree top
detection and crown delineation**

Nina Amiri
February, 2014

Course Title: Geo-Information Science and Earth Observation for
Environmental Modelling and Management

Level: Master of Science (MSc)

Course Duration: August 2012 – March 2014

Consortium Partners:

Lund University, (Sweden)
University of Twente, Faculty of ITC (The Netherlands)
University of Southampton, (UK)
University of Warsaw, (Poland)
University of Iceland, (Iceland)
University of Sydney, (Australia, Associate partner)

Assessment of Marker-Controlled Watershed segmentation algorithm for individual tree top detection and crown delineation

By

Nina Amiri

This thesis submitted to the Faculty of Geo-Information Science and Earth Observation of the University of Twente in partial fulfilment of the requirements for the degree of Master of Science in Geo-information Science and Earth Observation, Specialisation: Environmental Modelling and Management.

Thesis Assessment Board

Prof. Dr. Andrew K. Skidmore (Chair)
Dr. Valentyn A. Tolpekin (Externat Examiner)

Dr. Yousif Ali Hussin (First Supervisor)
Dr. Tiejun Wang (Second Supervisor)



UNIVERSITY OF TWENTE.

ITC

FACULTY OF GEO-INFORMATION SCIENCE AND EARTH OBSERVATION

Disclaimer

This document describes work undertaken as part of a programme of study at the Faculty of Geo-Information Science and Earth Observation of the University of Twente. All views and opinions expressed therein remain the sole responsibility of the author, and do not necessarily represent those of the institute.

Abstract

Light Detection And Ranging (LiDAR) technology has reached to the point where forest canopy height models can be produced at high spatial resolution. Individual tree crown isolation and classification methods are developing rapidly for multispectral imagery. Analysis of multispectral imagery, however, does not readily provide accurate tree height information and LiDAR data alone cannot provide tree attributes. In this regard, the combination of LiDAR and multispectral data at individual tree level could provide a very useful forest inventory tool. It is well known that the small gaps between tree crowns, branches and tree shadows normally cause over-segmentation when a Marker-Controlled Watershed segmentation approach is used to do the tree crown delineation. In order to eliminate such over-segmentation, in this study an ancillary data layer, i.e., NDVI was proposed in combination with high resolution multispectral imagery and LiDAR data for a better estimation of the individual tree top detection and crown delineation using Gaussian filtering and Marker-Controlled Watershed segmentation. To do so, we first defined a geographic object-based segmentation algorithm (i.e., Marker-Controlled Watershed segmentation); then we applied this algorithm for both very high resolution multispectral imagery and canopy height model created from a high point density LiDAR data over three subset areas with different forest canopy cover densities. Results show that automatic tree crown delineation based on the combination of multispectral imagery, LiDAR data and NDVI achieved an accuracy of 65.3%, which is significantly higher ($\chi^2(1,101)=0.016, p=0.05$) than the accuracy derived from the combination of multispectral and LiDAR data (61.7 %) in sparse forests. However, the significant accuracy improvement for tree crown delineation did not successful for the dense forests because of more serious commission errors. Our study demonstrated the importance of vegetation index (NDVI) in reducing the tree shadow effect in the sparse forest and thereby increasing the accuracy of tree crown delineation. Further work is needed to test our method in different types of forest ecosystems and under different topography conditions.

Acknowledgements

I would like to express sincere gratitude to my first supervisor Dr. Yousif Hussin, Natural Resources Department at ITC, University of Twente for his guidance and providing me an opportunity to work on this topic. I would like to express sincere gratitude to Dr. Tiejun Wang, Natural Resources Department at ITC, University of Twente, my second supervisor who has been very helpful and has assisted me in numerous ways during my thesis, who gave me a bright direction and motivation all the time to complete my research.

I would like to thank Prof. Andrew Skidmore for his cooperation, valuable inputs and suggestions in my research.

My special thanks and appreciation goes to Miss Anahita Khosravipour. Her valuable inputs and supports were vital for successful completion of my master thesis.

I would like to thank Dr. Kouros Khoshelham for his kind cooperation and support which also helped me in my thesis.

I would like to thank the European Commission, Erasmus Mundus Program, to give me a chance to study at Lund University, Sweden and the ITC, University of Twente, the Netherlands.

I would also like to thank my family, classmates and friends for all of their advices and encouragements during the thesis.

*“Research is to see what everybody else has seen,
and to think what nobody else has thought.”
Albert Szent- Györgyi*

Table of Contents

Abstract	v
List of figures	viii
List of tables	x
Chapter 1	1
1.1 Introduction	1
1.1.1 Background	1
1.1.2 Individual tree top detection and crown delineation segmentation algorithms.....	4
1.1.3 Vegetation index	6
1.1.4 Problem statement	8
1.1.5 Research Objectives.....	11
1.1.6 Research Questions	11
1.1.7 Research Hypothesis	11
1.1.8 Thesis Outline	12
Chapter 2	13
2.1 Materials and Methods.....	13
2.1.1 Study area	13
2.1.2 Materials.....	14
2.1.3 Methods.....	16
Chapter 3	33
3.1 Results.....	33
3.1.1 Crown delineation with GeoEye-2 imagery	33
3.1.2 Crown delineation with LiDAR data.....	36
3.1.3 Crown delineation with integration of GeoEye-2 imagery and LiDAR data	38
3.1.4 Crown delineation with integration of GeoEye-2 imagery and LiDAR data	39
3.1.5 Comparison of the four techniques in low, medium and high density canopy cover subset areas	42
Chapter 4	47
4.1 Discussion	47
Chapter 5	51
5.1 Conclusions and recommendations	51
5.1.1 Conclusions.....	51
5.1.2 Recommendations	52
References.....	53
Appendices	64

List of figures

Figure 1, Hills or mountains are canopy of trees and the valleys are the distances between the canopy in region-growing and valley-following algorithms.	6
Figure 2, Vegetation spectral responses, (Ashraf <i>et al.</i> , 2011).	7
Figure 3, Problem of light illumination in very high resolution satellite imagery to detect the appropriate tree top.	9
Figure 4, Shadows of trees, a) Individual tree on aerial photo, b) Individual tree canopy boundary emphasized by yellow line on CHM (Canopy Height Model) extracted from LiDAR and c) Individual tree canopy boundary on aerial photo with yellow line and shadow effect.	10
Figure 5, Field photograph of study area, Bois noir forest, Barcelonnette, South France.	13
Figure 6, The location of the study area, true colour composite of GeoEye-2 multispectral imagery obtained in 2012.	14
Figure 7, Sample waveform returns from vegetation and submerged topography (Wright and Brock, 2002).	15
Figure 8, Workflow of methods for individual tree top detection and crown delineation by Marker-Controlled Watershed algorithm, part 1.	17
Figure 9, Workflow of methods for individual tree top detection and crown delineation by Marker-Controlled Watershed algorithm, part 2.	18
Figure 10, The location of three subset area plots (low, medium and high density of forest canopy cover).	19
Figure 11, Scatter plot of subset areas present the position and distribution of plots.	20
Figure 12, Statistics plots of pan sharpened GeoEye-2.	22
Figure 13, 3D visualization of a single tree from LiDAR point cloud.	24
Figure 14, a) DTM (Digital Terrain Model), b) DSM (Digital Surface Model), c) CHM (Canopy Height Model) in 3D view and d) Intensity (measure of the return strength of the laser pulse).	25
Figure 15, Normalized Difference Vegetation Index (NDVI) layer of the study area and the location of subset areas for June 2012.	26
Figure 16, Watershed segmentation grey level profile of image data, local minima of grey level yield catchment basins, local maxima define the Watershed lines.	28
Figure 17, The 3 by 3 kernel of Sobel filter (edge detection) in 2 directions.	28
Figure 18, Morphological techniques, erosion and dilation for the background markers.	29

Figure 19, Steps of Marker-Controlled Watershed segmentation algorithm with morphological techniques.	29
Figure 20, a) Perfect match, b) Good match, c) Split d) Omission and e) Commission. Yellow polygons are ground reference crowns and green polygons are segmentation algorithm results.....	31
Figure 21, Input data methods for extracting individual crowns.	33
Figure 22, Statistical accuracy histogram of individual tree crown delineation versus ground reference crowns based on multispectral imagery.....	34
Figure 23, An example of tree crown segmentation for the single plot in the low density subset area. Red polygons are ground reference crowns and cyan polygons are algorithm results.	35
Figure 24, Statistical accuracy histogram of individual tree crown delineation versus ground reference crowns based on LiDAR data...	36
Figure 25, An example of tree crown segmentation for the single plot in the low density subset area. Red polygons are ground reference crowns and cyan polygons are algorithm results.	37
Figure 26, Statistical accuracy histogram of individual tree crown delineation versus ground reference crowns based on the multispectral imagery and LiDAR data integration.	39
Figure 27, An example of Crown delineation on low density subset area by Marker-Controlled Watershed segmentation on GeoEye-2, CHM and NDVI integration. Red polygons are ground reference crowns and green crowns are segmentation algorithm results.	41
Figure 28, Statistical accuracy histogram of individual tree crown delineation versus ground reference crowns based on the multispectral imagery, LiDAR data and NDVI integration.....	41
Figure 29, Statistical accuracy histogram of individual tree crown delineation versus ground reference crowns for the low density subset area.	44
Figure 30, Statistical accuracy histogram of individual tree crown delineation versus ground reference crowns for the medium density subset area.....	45
Figure 31, Statistical accuracy histogram of individual tree crown delineation versus ground reference crowns for the high density subset are.	46

List of tables

Table 1, LiDAR metadata	15
Table 2, The spectral range of GeoEye-2 imagery	16
Table 3, Correlation across GeoEye-2 spectral bands.....	22
Table 4, Correspondence of individual tree crown delineation versus ground reference crowns based on multispectral imagery	34
Table 5, Correspondence of individual tree crown delineation versus ground reference crowns based on LiDAR data	37
Table 6, Correspondence of individual tree crown delineation versus ground reference crowns for multispectral imagery and LiDAR data integration.....	38
Table 7, Summary of statistical test for samples from LiDAR based data segmentation versus GeoEye-2 imagery and LiDAR integration	39
Table 8, Correspondence of individual tree crown delineation versus ground reference crowns for multispectral imagery, LiDAR data and NDVI integration.....	40
Table 9, Summary of statistical test for segmentation results of Geoeeye-2 imagery, LiDAR based vs. GeoEye-2 imagery, LiDAR and NDVI based in low density subset area	42
Table 10, Summary of statistical test for segmentation results of Geoeeye-2 imagery, LiDAR based vs. Geoeeye-2 imagery, LiDAR and NDVI based in medium density subset area	43
Table 11, Summary of statistical test for segmentation results of Geoeeye-2 imagery, LiDAR based vs. Geoeeye-2 imagery, LiDAR and NDVI based in high density subset area	43
Table 12, Correspondence of individual tree crown delineation versus ground reference crowns for low density subset area	44
Table 13, Correspondence of individual tree crown delineation versus ground reference crowns for medium density subset area	45
Table 14, Correspondence of individual tree crown delineation versus ground reference crowns for high density subset area	46

Chapter 1

1.1 Introduction

1.1.1 Background

Individual tree structure and crown concentration are the important factors for suitable forest management and inventory purposes (Gougeon, 1998). Conventionally, this information collected by means of field surveys. Such surveys were time consuming and expensive process when carried out over broad areas (Brown *et al.*, 1989). The essential requirements of the present-day forest inventory are the accurate and continuously updated resource data of forest covers. Remote sensing seems to be a valuable and low-cost tool for determining individual tree characteristics and attributes when compared to field surveys (Ozdemir and Karnieli, 2011).

Extraction of individual trees structure information by remote sensing have significant implications in the forest applications (Chen *et al.*, 2006). As an example, primary step for isolation of individual tree crowns is relevant tree structure factors. To obtain this first individual tree top should be defined and then crown boundary delineated. Estimating precise crown segmentation is a challenging task, because of the irregularity in many crown boundary shapes and difficult to measure them by using standard forestry field equipment (Kato *et al.*, 2009). In addition, accurate isolation of individual tree crown because of within crown shadows and gaps is difficult (Dorren *et al.*, 2003). Therefore, comprehensive research by remotely sensed data has been done on systematic of tree top detection and crown delineation.

Earlier low resolution (e.g., 30 meters) remotely sensed data were not suitable for individual tree crown delineation, because of the pixel size which is usually much bigger than a typical tree crown size. Strahler *et al.*, (1986) because of the object size importance mentioned a necessary factor for segmentation purposes which is the spatial resolution of these images. Because of the low spectral resolution of earlier remote sensing data, a sufficient amount of work for extracting tree crowns was based on aerial photos with high resolution (Brandtberg and Walter, 1998). Automatic tree crown delineation from aerial photos requires a pixel size much smaller than the crown size to recognize the tree and define the crown boundary. However, high spatial resolution imagery increasing the within-crown

brightness variation and making the tree crown identification difficult (Song *et al.*, 2010). Process of detection often presumes that each tree has a boundary with no overlap between mixed crowns, but overlap is the common measurement problem in a real forest condition (Song *et al.*, 2010). Therefore, researches show that direct delineation of tree crowns on high spatial resolution aerial photos can lead to significant errors in both, the number of crowns and the crown size (Brandtberg and Walter, 1998).

With the significant improvements in spatial resolution of satellite imagery during the last decades, researchers have begun to explore application of satellite data for estimating forest canopy structure (Amiri, 2013). The increasing availability of data from high spatial resolution satellites for example, IKONOS, QuickBird, WorldView and Geo-Eye provides a wider broadening view compared to aerial photographs and low resolution images (Gougeon, 2003). The very high resolution (VHR) satellite images provide spectral signature of the individual tree canopies as objects which make a shift from traditional pixel-based techniques towards the object-based methods for delineation of tree crowns (Gougeon & Leckie, 2006). However, an important limitation in the forest inventory studies still remains; the lack of high geometric details (peaks and valleys) to explain the height, structure and size of crowns (Zhang and Hu, 2012). The similarity of spectral signatures for different tree species, as well as assemblage of tree crowns with little to no inter crown distance and occurrence of overlapping in crown canopies, increase the challenges for successful tree cover identification from high resolution remote sensing data (Ghosh *et al.*, 2014).

The increasing availability of the Light Detection And Ranging (LiDAR) data has been provided a new source for individual tree detection and crown cover delineation (Hyypä *et al.*, 2004). The high sampling LiDAR point cloud can provide species-specific vertical crown structure (Ke *et al.*, 2010). In recent years, LiDAR data has emerged as a new source for forest inventory analysis, especially for individual tree detection and crown isolation (Beuning *et al.*, 2004; Hyypä *et al.*, 2004). Compared with passive remote sensing, LiDAR has the advantage of directly measuring the 3 dimensional coordinates of canopies. Therefore, the geometric properties, "peaks" and "valleys" rather than spectral, can be detected (Chen *et al.*, 2006). Numerous studies have focused on methods developed from optical imagery and aerial photos to LiDAR technology for individual tree analysis (Hyypä *et al.*, 2001; Koch *et al.*, 2006). Brandtberg *et al.*, (2003) extended the scale-space theory to detect crown segments. Chen *et al.*, (2006) to reduce the over-segmentation problems applied the Marker-

Controlled Watershed algorithm to LiDAR active remote sensing. However, the studies have shown that over-estimation problems still remain (Kim *et al.*, 2010).

The advantage of LiDAR data coincided with fine resolution multispectral satellite imagery provide new methods for individual tree segmentation (Ørka *et al.*, 2012). This technology in combination with high spatial resolution optical imagery (e.g., ground sample distance (GSD) ≤ 4 m) becomes more available, therefore the applications for detailed forest inventory has been increased (Ke *et al.*, 2010). As an example, Ke *et al.*, (2010) combined low point-density LiDAR data and Quickbird image for forest species classification using an object-based approach and has resulted in high identification accuracy with the Kappa of 0.91. In the case of individual tree classification, the information on the vertical structure of individual trees from the LiDAR data complements the spectral information from the optical imagery (Gougeon, 2003). Leckie *et al.*, (2003) applied the valley-following segmentation algorithm based on digital camera imagery into the LiDAR data. They found, LiDAR can easily eliminated most of the commission errors that occur in the open stands with optical image, whereas the optical image produced a better isolation in the more dense stands. They claimed a complementarity in the two data sources that will help tree isolation. While LiDAR offers high geometric details and VHR optical imagery spectral signatures, the lack of accurately detection and delineation of crown boundaries still remains as an important limitation of forest inventory studies because of the within crown shadows and other materials (King *et al.*, 2002).

For automatic tree top detection and crown delineation, segmentation algorithms may be an effective means to accomplish accurate tree crown delineation. Since the segmentation algorithms were developed for specific site conditions, used different types of imagery and evaluated with different accuracy assessment approaches, it is difficult to compare their performances (Ke and Quackenbush, 2011). However, improving the current methods and algorithms for crown delineation and detection by ancillary data could become suitable for different forest conditions and image types. A framework of Marker-Controller Watershed segmentation is proposed in this study to improve the delineation of crown covers by integration of the VHR satellite imagery, LiDAR data and NDVI (Normalized Difference Vegetation Index) to avoid within-crown shadows.

1.1.2 Individual tree top detection and crown delineation segmentation algorithms

Object-based segmentation techniques have been proposed to combine the visual interpretation context with the pixel-based methods for crown cover delineation (Desclee *et al.*, 2006). The improvements in image processing techniques and segmentation algorithms has increased the interest for object-based methods for forest inventory applications (Mäkelä and Pekkarinen, 2001). The main advantage of object-based methods is the incorporation of contextual information in the forest inventory and delineation analysis (Flanders *et al.*, 2003). These methods allow the segmentation and extraction of semi-automated crown covers from remote sensing data and also facilitates the integration of raster-based processing and vector-based (Blaschke, 2010). Currently there is a growing interest among researchers in finding segmentation methods to combine data from different sources and obtain information that no single source can provide individually.

The history of studies on automatic crown detection and delineation algorithms from digital imagery dates back to the mid-1980s. One of the earliest examples was the research of Pinz, (1991) using the Vision Expert to locate the center of a crown and estimate the radius by searching for local brightness maxima in smoothed aerial images with a 10 cm pixel size. In the mid-1990s, Gougeon, (1995) presented a valley-following and rule-based algorithm to fully delineate coniferous tree crowns by following the valleys of shadows between tree crowns using 36 cm ground sampled distance (GSD) on digital aerial imagery (Ke and Quackenbush, 2011). During the same time, to estimate the area occupied with a tree crown, multiple scale analysis was applied on higher resolution satellite imagery (Brandtberg and Walter, 1998). Then model-based template matching techniques were introduced to recognize individual trees (Pollock, 1996). Later, Gougeon, (2003) divided these approaches into three different categories based on the type of information being extracted: tree location detection, tree location detection and crown dimension parameterization, and full crown delineation (Ghosh *et al.*, 2014). Therefore, in most of the segmentation methods crown detection is an important step before crown delineation.

The accuracy of tree top detection process significantly influenced the accuracy results of crown delineation (Ke and Quackenbush, 2011). Therefore, the algorithms can be divided in to two general steps in terms of their purpose: tree top detection and crown delineation algorithms. Tree top detection defined as a process that deals with

finding the tree tops or accurate geometric location of trees. Tree crown delineation focused on automatically defining crown ridges. Therefore, tree identification and top detection is not only as a aim by itself, but also as a necessary pre-processing step for accurate crown delineation or dimension determination (King *et al.*, 2002; Ke *et al.*, 2010).

Tree top detection methods have focused on the identification of local maxima using (1) enhancement and thresholding (Wulder and Franklin, 2003), where a global image operation such as smoothing or high-pass filtering is applied and the resulting pixel brightness values within a defined range are extracted as tree locations. (2) Template matching (Pollock, 1998), introducing the correlation between the geometric-radiometric model of a tree crown and image data. (3) In Multiscale analysis (Brandtberg and Walter, 1998), the occurrence of edges over several scales is tested to define a approximate region in which the brightest pixel value is taken as a top for tree. (4) Local maxima filtering (Culvenor *et al.*, 1998; Wulder *et al.*, 2000), where the maximum pixel brightness value in a kernel sample with a specified size which is taken to represent the tree top.

Crown delineation algorithms have been accomplished by (1) Outlining a network of minimum image values, known as valley-following (Gougeon, 1995) which found local minima as valley bottoms. Valleys were defined by searching for adjacent pixels that were between pixels with higher values. The valley extraction often showed incomplete separation of tree clusters due to branches extending in to neighbourhood crowns (Ke and Quackenbush, 2011). (2) Region-growing, involving the identification of groups of similar neighbouring pixels. The region-growing algorithm developed by Horowitz and Pavlidis in 1976 (Jain, 1989). The algorithm is an image segmentation approach used to separate homogenous regions and recognize objects in an image. In order to keep the background interruption away, users need to provide highest points and the criteria to stop growing process (Ke and Quackenbush, 2011). Region-growing has been widely used for feature extraction in computer vision (Gonzalez and Woods, 2007). Figure 1, shows the basic concepts of two mentioned crown delineation approaches (adapted from Culvenor, 2002). 3) Watershed segmentation algorithm, based on the grey-level image definition as a topographic surface where the digital value for each pixel can be signed as the elevation at that point. In the watershed segmentation, the image grey tone is inverted so the local maxima become local minima and vice versa (Ghosh *et al.*, 2014). To avoid the over-segmentation problem due to the noise on image, Beucher, (1990) introduced

Marker-Controlled Watershed segmentation. Wang *et al.* (2004) detected tree tops as markers within each object by morphological techniques and applied Marker-Controlled Watershed segmentation to the geodetic distance image that was generated from the tree crown objects image.

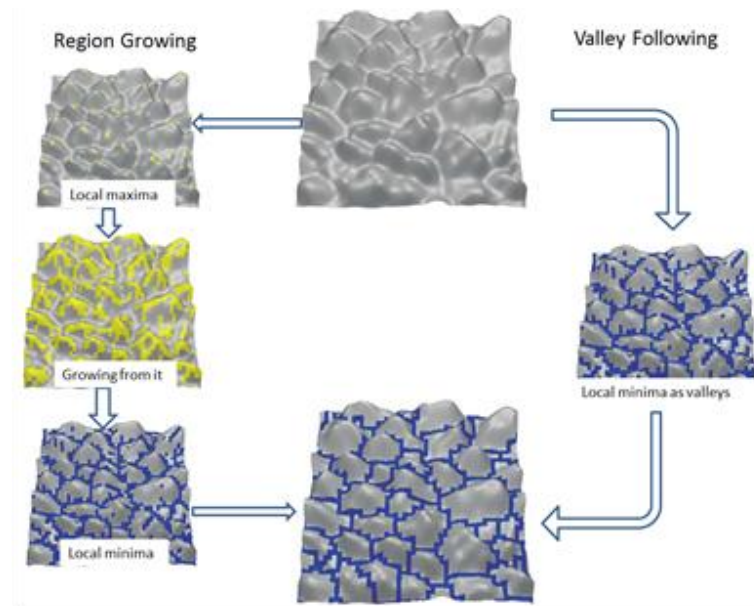


Figure 1, Hills or mountains are canopy of trees and the valleys are the distances between the canopy in region-growing and valley-following algorithms (Culvenor, 2002).

1.1.3 Vegetation index

The multispectral remote sensing images carry essential integrating spectral and spatial features of objects (Bhandari *et al.*, 2012). Digital image processing of satellite data provides tools for analysing the data through the different algorithms and mathematical indices to extract objects. The use of appropriate additional data layer also helps to quantify the variables of interest in the object-based segmentation algorithms. The differences between the visible red and near-infrared bands of multispectral image can be used as an indicator for the areas containing significant vegetation and other different objects (Gutman, 1991).

Numerous studies have assessed the potentials of ancillary data to the individual crown delineation results by incorporating it with

topography information (Hutchinson, 1982; Ricchetti, 2000), spectral derived texture (Chica-Olmo and Abarca-Hernandez, 2000; Li and Eastman, 2006) and radar derived texture (Dong and Leblon, 2004; Mather *et al.*, 1998). Brenning, (2009) described an application to improve mapping accuracy by combining process of terrain attributes derived from digital elevation model and multispectral Landsat TM/ETM+ (Willers *et al.*, 2012). He found that the integration of terrain attributes and multispectral imagery is necessary for mapping activity. Jiang *et al.*, (2011) and Koetz *et al.* (2008) described applications where the goal of the integration of data layers was to improve the classification accuracy of the imagery. The LiDAR data or multispectral imagery data derived products, when used separately (Willers *et al.*, 2008) provide some useful information about an individual tree crown. The topography variable or NDVI derived from a multispectral imagery may provide a significant improvement in the segmentation results (Grebby *et al.*, 2011).

Remotely sensed vegetation indices such as NDVI are widely used and have numerous benefits in the assessment of forest inventory. Vegetation indices are intended to enhance the vegetation signal, while trying to minimize the solar irradiance and soil background effects. Although these indices were developed to extract the chlorophyll signal only, the soil background, moisture condition, solar zenith angle, view angle, as well as atmosphere, alter the values (Jackson and Huete, 1991). However, the NDVI have been used widely to investigate the relation between spectral variability and the vegetation or growth rate in the forestry (Bhandari *et al.*, 2012). Figure 2 shows the spectral responses of vegetation in different bands.

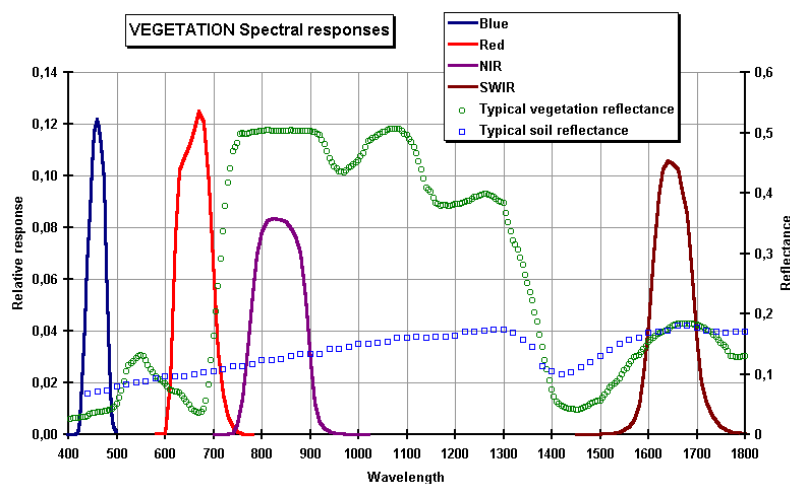


Figure 2, Vegetation spectral responses, (Ashraf *et al.*, 2011).

The NDVI indicator defined by relation between the absorption of red radiation by vegetation chlorophyll and the strong scatter of near-infrared radiation (Beck *et al.*, 2006). NDVI helps to explain the variability in crown delineation as well as health of forests (Mohan *et al.*, 2009; Tiruveedhula *et al.*, 2009). Also, multispectral data from near nadir view angle gives the maximum value for NDVI (Gutman, 1991). The main advantage of NDVI is to have the inherent nonlinearity of a ratio-based indices (Maskova *et al.*, 2008). Branches, tree crown shadows, and tree clusters are usually have similar shapes and overlapping sizes which cause low accuracy on the current techniques of segmentation (Hu *et al.*, 2014). The idea of using NDVI as an ancillary data is to improve effectively the delineation of crown cover segmentation. Also, compare the different crown delineation algorithms based on their advantages and limitations with focus on data integration may open the space for more developments to improve the accuracy.

1.1.4 Problem statement

Over the last two decades, a large variety of tree top detection and crown delineation algorithms has been processed and developed. The advantages/disadvantages of a particular method can greatly affect the result of tree top detection and crown delineation; therefore a specific application could affect the descriptive parameters (crown attributes). Even though, in the same environment, different purposes may yield to different results. Therefore, the selection of an appropriate algorithm which is significantly acceptable, mainly based on the approach (Ke and Quanckenbush, 2011).

The problem of tree top detection is related to the problem of finding the brightest peak in the very high resolution image, which means finding the pixel with maximum brightness value among the surrounding pixels (Heinzel *et al.*, 2008). In the very high resolution imagery light illumination affects the correct detection of the tree tops as it is shown in Figure 3. Moreover, the difficulty of crown boundary delineation related to the delineation of dark valleys, which are the pixels surrounding the boundary. The local spectral variation caused by crown textures, gaps, or shadows may affect crown delineation in very high resolution optical imagery. On the other hand, segmentation based on LiDAR point cloud requires an appropriate neighbourhood definition and the neighbours can be retrieved by the values of additional spectral attributes (Pfeifer *et al.*, 2013). The smoothing progress by image processing filters to reduce the measurement errors on the LiDAR based canopy surfaces; indeed alter the original structure of tree crown.

An integration approach although provides high interpretation capabilities and more reliable results but (structural) vertical LiDAR data and spectral have different data sources characteristics (Pohl and Van Genderden, 1998; Swatantran *et al.*, 2011). In this approach, some confounding factors related to the integration of geometry and spectral characteristics of the datasets may affect the process of extracting accurate crown boundaries (Willers *et al.*, 2012). These errors will affect the accuracy of crown cover segmentation for delineation purposes in forest inventory.

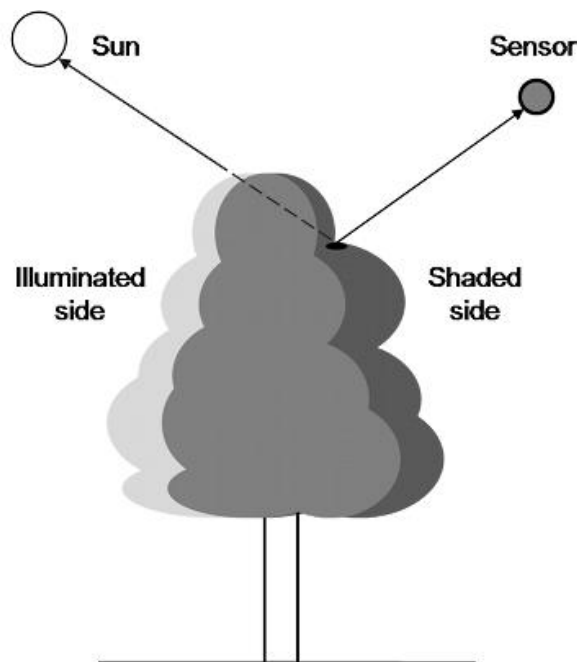


Figure 3, Problem of light illumination in very high resolution satellite imagery to detect the appropriate tree top (Kukunda, 2013).

As an example the high signal to noise ratio in optical satellite imagery affects the spectral quality of crowns by blurring the edges due to the light illumination and shadows affect (Figure 4). Blurring edges in optical imagery are due to refutation between spatial and spectral resolutions (Liu, 2000). In mountainous terrain surfaces of forests, topographic discontinuities and distortions also create blurring in optical imagery; containing from direct feature illumination shadows especially if the scene is taken during sunny conditions (Dorren *et al.*, 2003). The mentioned problem is not occur with high density LiDAR data, as the forest crown cover have very high

geometric precision and do not have shadows from light illumination (Figure 4).

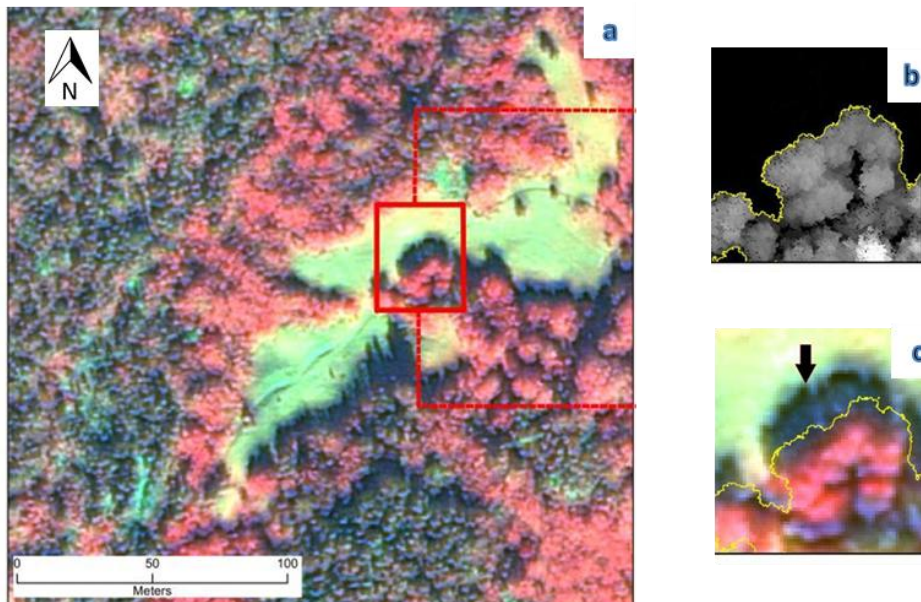


Figure 4, Shadows of trees, a) Individual tree on aerial photo, b) Individual tree canopy boundary emphasized by yellow line on CHM (Canopy Height Model) extracted from LiDAR and c) Individual tree canopy boundary on aerial photo with yellow line and shadow effect (Kukunda, 2013).

The soil background of forest will influence the individual crown delineation results as it is not fully covered by vegetation (Jackson and Huete, 1991). For incomplete canopies, the background soil in shape of gaps and shadows will cause a change in the results. The change is further complicated by the fact of light transmission through the vegetation in denser canopies. Forest canopy surfaces are non-lambertian. The light reflected from these surfaces which is the main source of shadow is highly dependent on view and solar angle. View and solar angle affection on radiation reflected from the surface (Pinter *et al.*, 1983) is not the focus of this study. These angles effect as shadows on the canopy surface could reduce the accuracy of tree top detection and crown delineation. Huete and Warrick, (1990) denoted that this effect of background successfully could minimize by using ground based and satellite data (Huete and Warrick, 1990).

This study explores two approaches, first to conduct a detailed assessment and evaluation on tree top detection and crown delineation algorithm, Marker-Controlled Watershed segmentation, with integration of GeoEye-2 multispectral satellite imagery and high point density LiDAR data. Secondly, to contribute the Marker-Controlled Watershed segmentation by NDVI to improve the accuracy of crown delineation based on integration of GeoEye-2 multispectral imagery and LiDAR data.

1.1.5 Research Objectives

The research objectives of this study are:

To evaluate the performance of the Marker-Controlled Watershed segmentation algorithm for tree top detection and crown delineation using GeoEye-2 multispectral satellite imagery and high resolution LiDAR data.

To assess the contribution of NDVI to the overall accuracy of the Marker-Controlled Watershed segmentation algorithm in tree crown delineation using GeoEye-2 and LiDAR data.

1.1.6 Research Questions

Research question are:

- Is there a statistically significant difference in accuracy for tree crown delineation by the Marker-Controlled Watershed segmentation algorithm with different inputs of data?
- Is there a statistically significant difference in the accuracy for tree crown delineation with and without the use of NDVI?

1.1.7 Research Hypothesis

Research hypothesis based on research objectives described below:

Hypothesis 1

H0: There is no statistically significant difference in accuracy for tree crown delineation between the different data inputs for the Marker-Controlled Watershed segmentation algorithm.

H1: The LiDAR, multispectral data combination statistically produces a significantly higher accuracy for tree crown delineation than the use of each input data individually.

Hypothesis 2

H0: There is no statistically significant difference in accuracy for tree crown delineation with and without consideration of NDVI as an ancillary data.

H1: Adding NDVI data to the integrated input data for tree crown delineation produces a statistically significantly higher accuracy than without consideration of NDVI.

1.1.8 Thesis Outline

This thesis is divided into five chapters. Chapter One introduces the study with a synthesis of advances, strengths, weakness, challenges and opportunities of the object-based segmentation methods, as well as the use of the LiDAR and VHR satellite imagery data in tree detection and crown delineation. Moreover, research problems, objectives, hypothesis are highlighted in this chapter. Chapter Two describes the study area, materials, methods and analysis undertaken to answer the research questions. In Chapter Three, the results of the research are presented, while they are discussed in Chapter Four. The research conclusions and recommendations are presented in Chapter Five.

Chapter 2

2.1 Materials and Methods

2.1.1 Study area

The study site is a forest area originally planted in early 19th century located in north-facing slope of the Barcelonnette, South France (Figure 5). The area has relatively homogenous forest stands, dominated mostly by two canopy layers based on two trees species. The area is about 1.3 square km and it is a part of a larger Bois noir Forest which is a French word and it means 'Black Wood'. The Barcelonnette Basin is representative of common climatic and land cover conditions for many regions of the South France Alps (Flageollet *et al.*, 1999). Weather stations provided daily information on rainfall, temperature and snow cover in Barcelonnette since 1928 (Flageollet *et al.*, 1999). The basin has a dry and mountainous (slope 10-35°) climate with strong inter-annual rainfall variability (e.g. annual rainfall may vary between 410 and 730 mm). Based on the rainfall records from 1928 till 2002 in the area, chances for strong storm rain intensities and 130 days of freezing per year exists (Maquaire *et al.*, 2003). The Bois noir is mostly covered by coniferous forest (76%) followed by bare land (9%) in the South Eastern part, broad leaved forest (6%) in the Northern part, pastures (6%), and natural grassland (3%) spread over the whole area (Kummar, 2009).

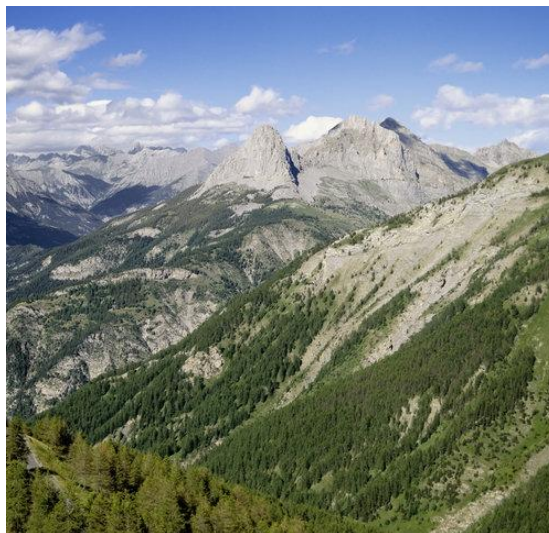


Figure 5, Field photograph of study area, Bois noir forest, Barcelonnette, South France (Panoramio, Google Maps, Gilly, 2012).

Over the years, the Bois noir forest has had minor silviculture and few studies have been published on the different aspects of the forest such as, tree density, diversity and composition. The field data which was collected in 2012 showed that mono-species stands of conifers dominant the study area with varied patches of mixed and broadleaved. Based on the results of field work, Scot pine (*Pinus sylvestris*) and Mountain pine (*Pinus uncinata*) are the dominant species of the Bois noir forest. Differences in forest structure have been reported to affect the derivation of forest metrics (Goodwin *et al.*, 2007; Lopez Saez *et al.*, 2011). Figure 6, presents the location of the study area.

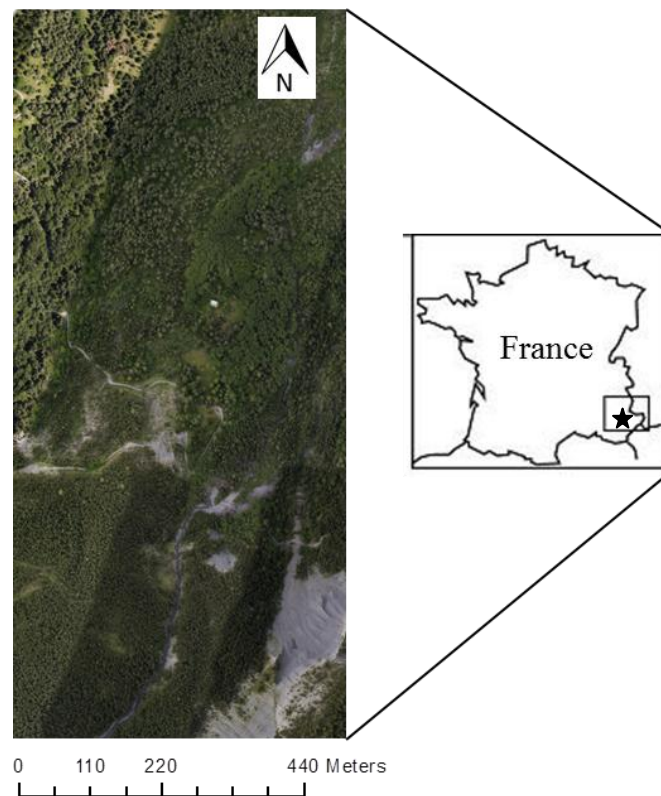


Figure 6, The location of the study area, true colour composite of GeoEye-2 multispectral imagery obtained in 2012.

2.1.2 Materials

The LiDAR and GeoEye-2 datasets were acquired during leaf-on, near nadir and snow free conditions in June 2009 and 2012 respectively. Table 1 presents additional metadata for the LiDAR dataset.

Table 1, LiDAR metadata

Measurement rate	Up to 150 000 s^{-1}
Beam divergence	0.3 mrad*
Laser beam footprint	75mm at 250 m
Field of view	60 degree
Scanning method	Rotating multi-facet mirror

* mrad is the unit of absorbed radiation dose.

LiDAR Data

The LiDAR dataset was collected primarily for a geomorphological study on the train model quality of the basin (Razak *et al.*, 2011). The data was collected by an airborne laser scanning system (Figure 7) mounted on a helicopter fly at 300m height above the ground by Helimap Company SZ. This company used the laser scanner system named as RIEGL VQ 480 with a pulse repetition rate up to 300 kHz to record the data. The spatial positioning was done using GPS and GLONASS positioning satellites. The orientation of the aircraft was determined by using the iMAR FSAS inertial measurement unit (IMU).

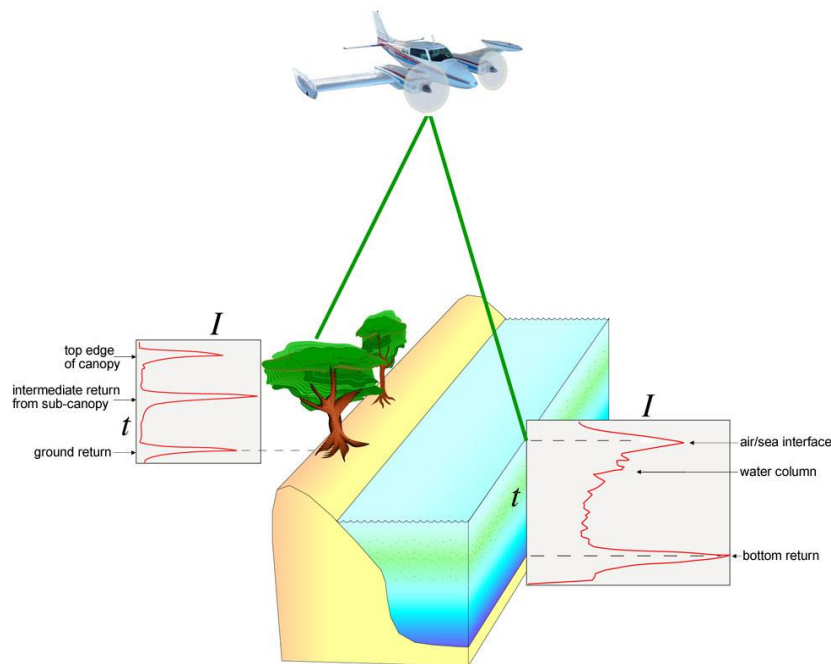


Figure 7, Sample waveform returns from vegetation and submerged topography (Wright and Brock, 2002).

In total, seven flight lines were achieved resulting into a cloud of 213.7 million points and very high mean density of 160 points per square meter. 113 points per square meter for all and last return recorded respectively. The LiDAR system recorded a maximum of five returns per pulse with the respective intensity (reflectivity) value. The point cloud was stored in LAS 1.0 format (Hug *et al.*, 2004) including four classes i.e. never classified (204 million points), unclassified (2926 points), ground (9.3 million points) and noise or low point (772 points).

GeoEye-2 Imagery

GeoEye-2 Imagery was acquired in June 2012 from IntraSearch Inc., MapMart, Colorado, USA, in GeoTIF format. This imagery was obtained during cloud free and near nadir conditions on the 26-6-2012. The acquired images with GeoEye-2 Satellite have the highest resolution of any commercial imaging system. It collected the images with a ground resolution of 34cm (13.4 inch) in the panchromatic or black-and-white mode and multispectral or colour imagery at 1.36-meter (54 inch) resolution (Satellite Imaging Corporation). Available data for this research has the 50 cm resolution in panchromatic band and 2 meters in multispectral bands. Table 1 presents the GeoEye-2 multispectral imagery spectral band ranges.

Table 2, The spectral range of GeoEye-2 imagery

<i>Spectral Range</i>	<i>nm</i>
Panchromatic	450 - 800 nm
Blue	450 - 510 nm
Green	510 - 580 nm
Red	655 - 690 nm
Near Infrared	780 - 920 nm

2.1.3 Methods

Workflow

Figure 8 and Figure 9, show the workflow for the objectives of this study in order to evaluate an object-based segmentation algorithm for crown delineation with integration of GeoEye-2 multispectral imagery and LiDAR data.

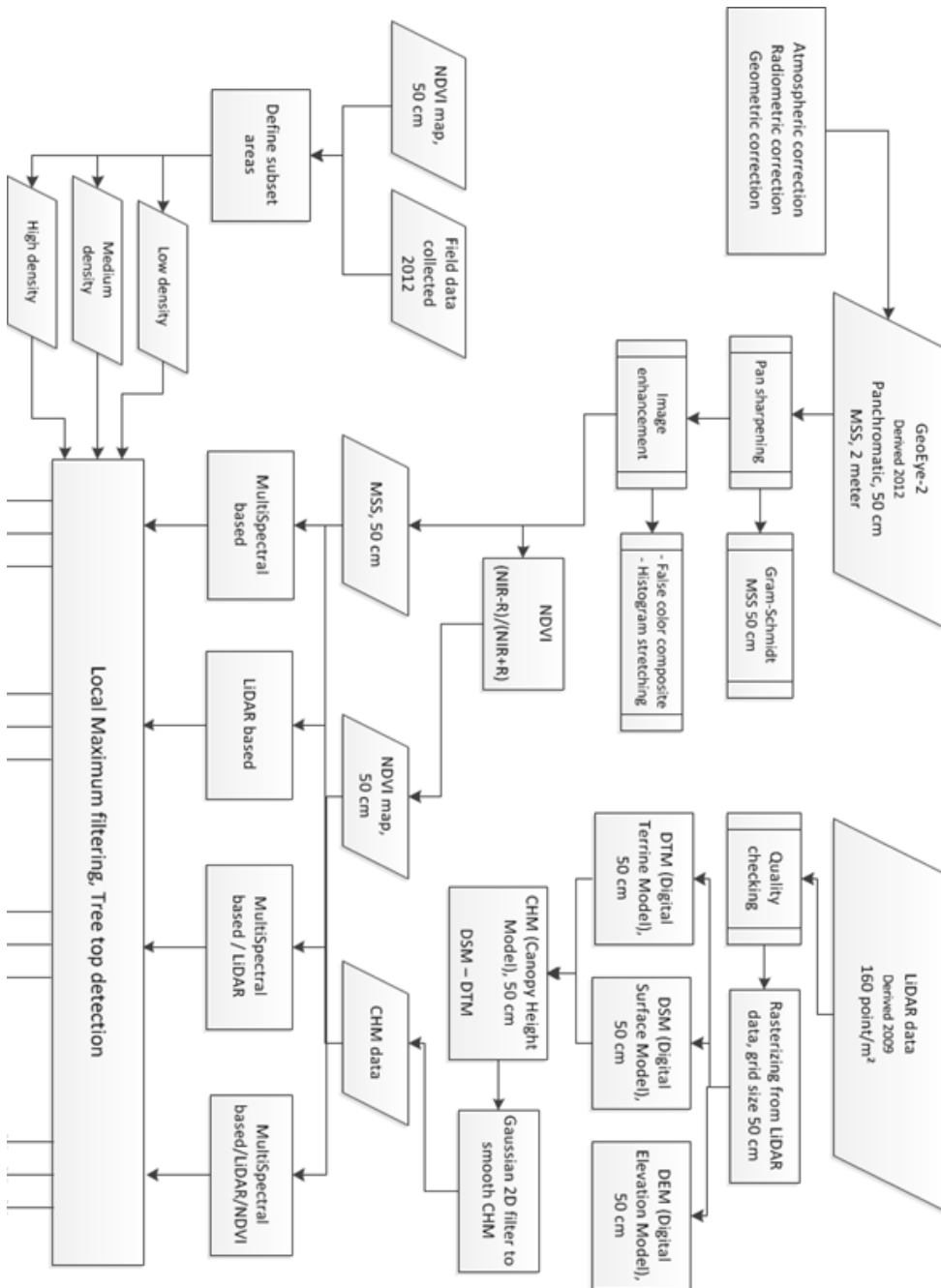


Figure 8, Workflow of methods for individual tree top detection and crown delineation by Marker-Controlled Watershed algorithm, part 1.

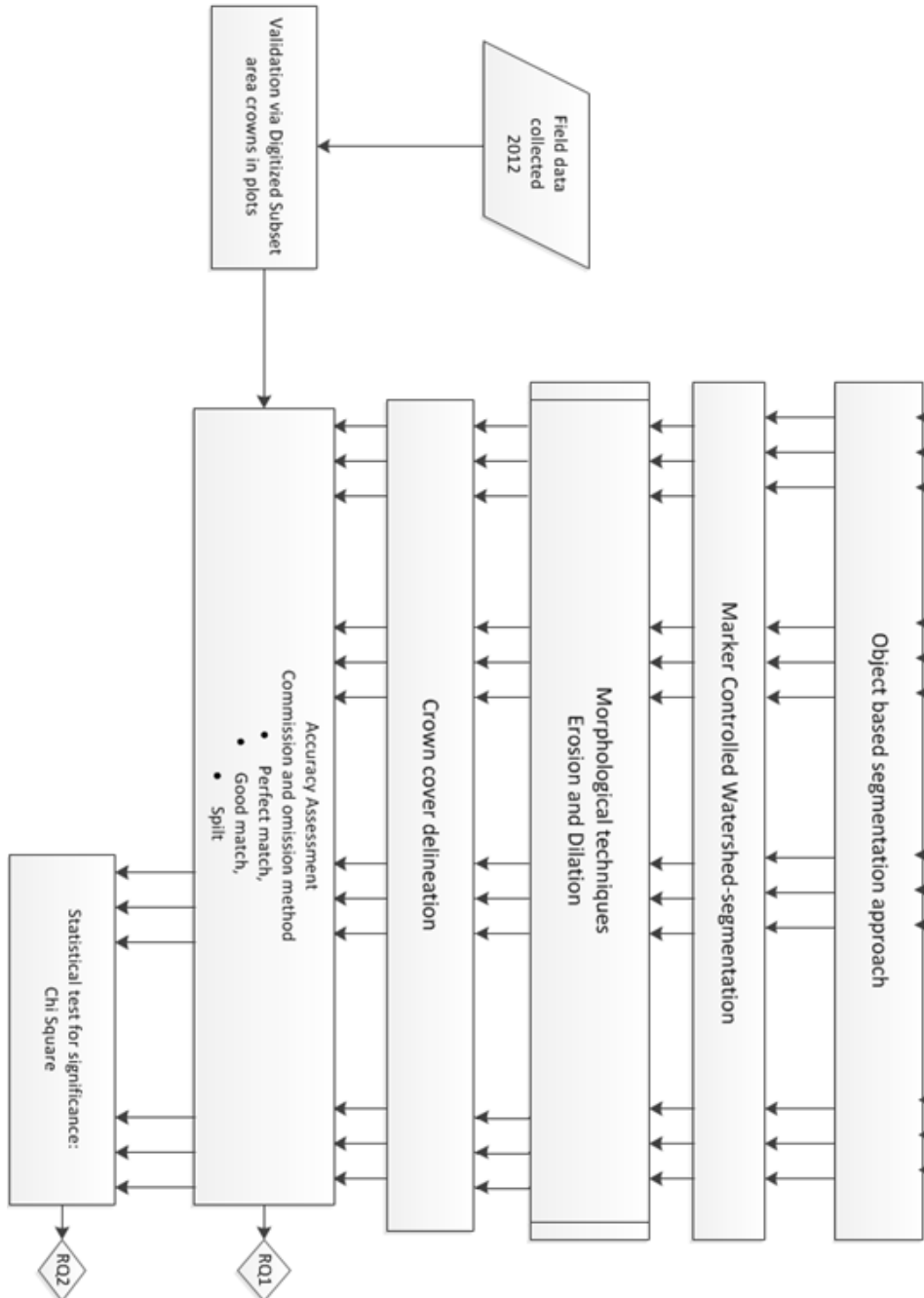


Figure 9, Workflow of methods for individual tree top detection and crown delineation by Marker-Controlled Watershed algorithm, part 2.

Data Collection

The field work data which is used in this study for validation purposes was collected during September 2012 (Kukunda, 2013). This time corresponded with the period of acquisition for the LiDAR with a 2 year lag and GeoEye-2 at the same year, respectively. The inter-date variability in the remote sensing data acquisition and field work was not a significant problem for this study (Ghosh *et al.*, 2014). This is because the forest exhibits a very slow growth rate explained by shallow soils along the slopes and it has a high tree density. Therefore, aside tree or branch fall due to the senescent and drunken nature of the area, the Bois noir's physical structure has remained unaltered. Figure 10 presents the location of subset areas in this study with different density of canopy cover.

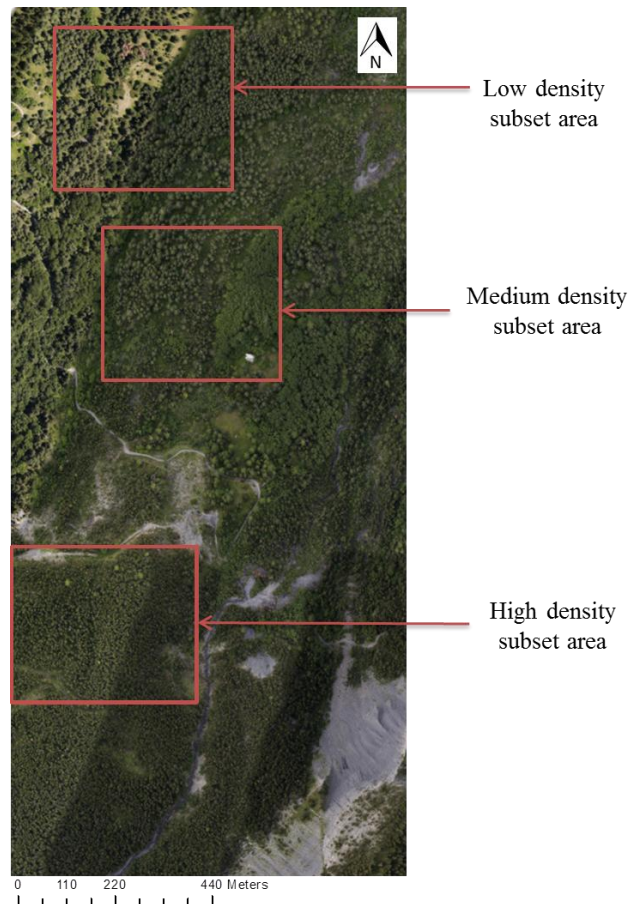


Figure 10, The location of three subset area plots (low, medium and high density of forest canopy cover).

Based on the properties of 2012 field work plots and NDVI map, three categories, low, medium and high density of forest canopy cover were selected to reduce the time of segmentation algorithm progress and to have an overview on canopy density factor effect after its implementation (Jovanovic *et al.*, 2011). Figure 11 shows the scatter plot of selected subset areas plot distribution. For validation purposes of this study for low density subset area 6 plots, for medium and high density 7 plots were selected.

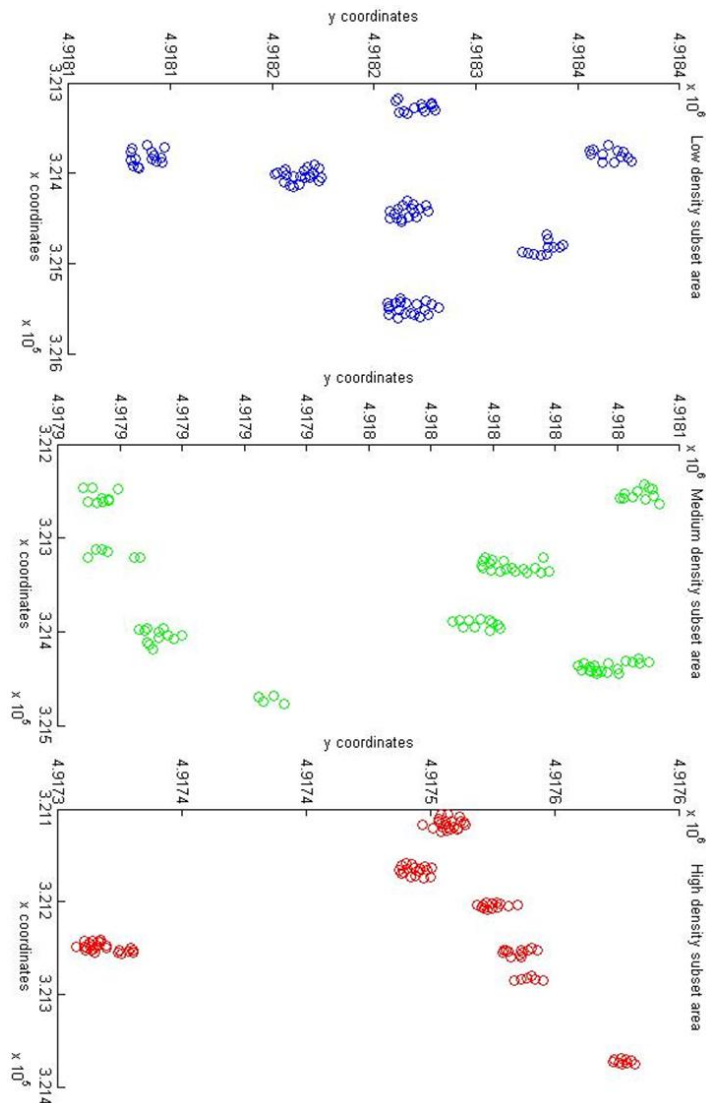


Figure 11, Scatter plot of subset areas present the position and distribution of plots.

GeoEye-2 Pre-processing

The GeoEye-2 imagery was delivered after atmospheric, radiometric and geometric correction by the IntraSearch Inc., MapMart. Image pre-processing involved two steps: pan sharpening and image enhancement.

Pan sharpening is an image fusion method originally to match the bands with lower resolution multispectral data with high resolution panchromatic band data to create a colorized high resolution dataset. The resulting product should only serve as an aid to literal analysis and not for further spectral analysis. For having an effective pan sharpening, the two images must be closely aligned. To accomplish this, tie points which marked the same features on both images are selected, then one image is warped to match the other based on these points.

In this study, the Gram-Schmidt pan sharpening method with 39 (GCP) Ground Control Points, nearest neighbour interpolation from polynomial methods in ENVI © 2008 software was used to sharpen the multispectral imagery (Jakubowski *et al.*, 2013). The Gram-Schmidt and PC (Principle Component) spectral sharpening tools both create pan sharpened images, but by using different techniques. Generally, the Gram-Schmidt method is more accurate than the PC method and is recommended for most of the applications (Maurer, 2013). Gram-Schmidt is typically more accurate because it uses the spectral response function of a given sensor to estimate what the panchromatic data look like. If we display a Gram-Schmidt pan sharpened image and a PC one, the visual differences are very subtle. The differences are in the spectral information by comparing Z-Profiles (spectral profiles) of the original image with the pan sharpened image, or calculate a covariance matrix for both images. The effect of pan sharpening is best revealed in images with homogenous surface features (flat deserts or water, for example) (Chavez *et al.*, 1991).

Image enhancement consist of false colour composite and histogram stretching. The bands selection for false colour composite based on the bands with high vegetation response information and correlation between the spectral values as shown in Figure 12 and Table 3. For composition purposes the least correlation between bands were selected from the tabel.

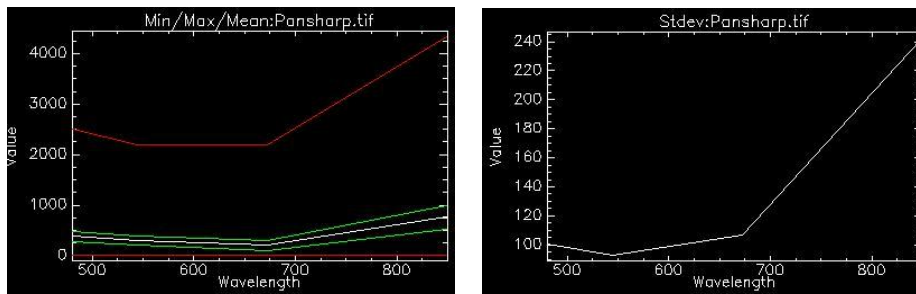


Figure 12, Statistics plots of pan sharpened GeoEye-2.

Table 3, Correlation across GeoEye-2 spectral bands

Correlation	Band1	Band 2	Band 3	Band 4
Band 1	1.000000	0.972	0.970	-0.04
Band 2		1	0.974	0.12
Band 3			1	-0.005
Band 4				1

LiDAR Pre-processing

LiDAR pre-processing consists of the quality checking, generation of the Digital Terrain (DTM), Digital Elevation (DEM), Digital Surface (DSM) and Canopy Height (CHM) models with 50 cm grid size. In this study LAsTools © software used for windows operating system.

Resolution of LiDAR surfaces

Point clouds are more often resampled to uniform grids in many forestry applications. Various surface interpolation methods are involved in the rasterization from LiDAR data (Reitberger *et al.*, 2009). The result cell size influences the quality of generated 2D-models. Too fine cell size, results to many 'no data' cells whereas too coarse cell size results to loss of details. The mean crown diameter measured in the field was 2.9 meters with the smallest crown at 50 cm diameter (Kukunda, 2013). Pouliot *et al.*, (2002) suggested to set the pixel size relative to the image object size. Therefore, a grid size of 50 cm chosen to match with the multispectral pan sharpened image and smallest crown size in the area falling within the ranged mentioned above.

Quality Checking of LiDAR

LiDAR is emerging as a fast and accurate technology for acquiring 3D coordinates of object space points at high density. The accuracy of the collected data depends on the data acquisition procedure and the calibration quality of the involved sub-systems (Abudal-Rahman *et al.*, 2006). This technology can be considered as a black box from the end user's perspective as the calibration process is not clear. Therefore, the users are left with quality control procedures as the only means for ensuring data integrity, correctness, and completeness (Abudal-Rahman *et al.*, 2006).

Habib *et al.*, (2008) defined "Quality control" as those steps necessary to ensure that delivered products satisfy client expectations for accuracy and utility. Since LiDAR data is always obtained by overlapping strips from different flight lines, a common quality control procedure is to check the coincidence of features in overlapping strips. The related algorithm in LAsTools © (Hug *et al.*, 2004) established the correspondence between overlapping LiDAR surfaces and estimates the transformation parameters (e.g., translations and rotations) related to them. For the final step of quality checking, the projection in Lambert conformal conic system based on the LiDAR airborne data's metadata defined and converted to UTM WGS84 zone 32N.

DTM, DSM, DEM and CHM Generation

Raster layers for both of the first return surface (digital surface model (DSM)) and bare Earth surface (digital elevation model (DEM)) were created from a triangular irregular network (TIN) (Suarez *et al.*, 2005) of the relevant data points at the same pixel size of the GeoEye-2 image (Ke *et al.*, 2010). In total, 9.4 million returns in the point cloud were classified as ground returns. The entire point cloud was delivered in 17 blocks, for easier management during rasterization, it is retilled to 13 blocks using the LAsTile © tool. In addition, for purpose of running the Marker-Controlled Watershed segmentation algorithm only subset areas selected. LAsGrid © tool was used to generate the DTM, keeping ground returns only and a fill of 2 pixels. The fill function determines the number of pixels to be considered in the prediction of 'no data' pixels based on the neighbouring during rasterization. Figure 13, shows a single tree 3D visualization derived from LiDAR point cloud.

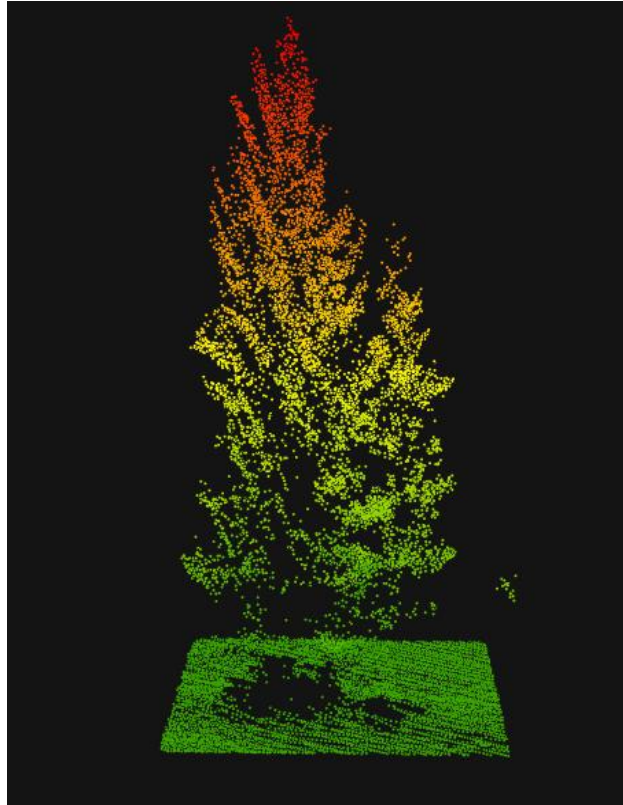


Figure 13, 3D visualization of a single tree from LiDAR point cloud.

For processing the point clouds and to generate the CHM (Canopy Height Model), we used the LASheight © tool while dropping all the noise points (i.e., point with height below -5 meters and above 60 meters). Extracting tree crown size by LiDAR data relies on the CHM, which is derived from subtracting the digital terrain model from digital surface model (Hu *et al.*, 2014). To smooth the CHM, make it more likely that each tree has a single height maxima and detect the tree top more accurate, 2D Gaussian filter (local maximum filtering) is used, where x and y is the distance to the kernel center. The location of trees is estimated by searching for local maxima height in the smoothed raster images (Persson *et al.*, 2002). The simplicity and advantage of using CHM oriented model is on the peak detection of the crown cover as geometric centroid (Hu *et al.*, 2014). Figure 14 shows a single subset area in DTM, DSM, Intensity of reflectivity and CHM visualization.

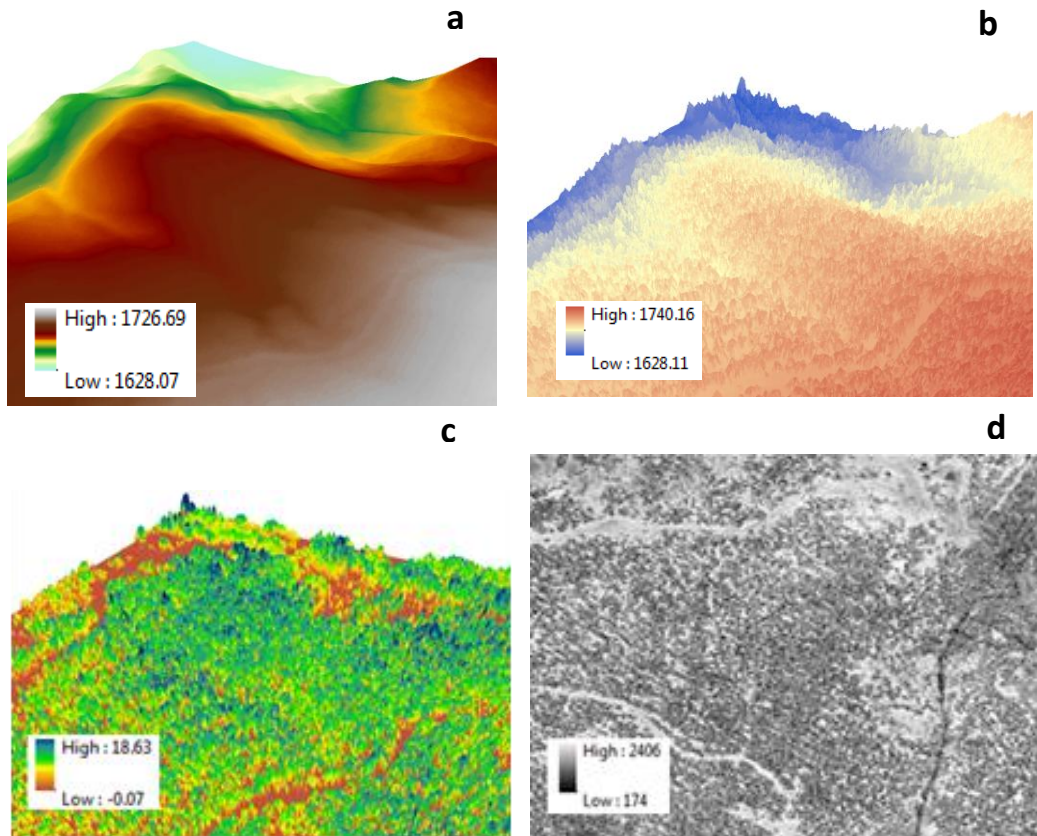


Figure 14, a) DTM (Digital Terrain Model), b) DSM (Digital Surface Model), c) CHM (Canopy Height Model) in 3D view and d) Intensity (measure of the return strength of the laser pulse).

NDVI

The NDVI dependent on the absorption of red radiation by chlorophyll of vegetation, and the scattering reaction of near-infrared radiation relation (Beck *et al.*, 2006). The NDVI is preferred for global vegetation monitoring because it helps to compensate the changing illumination conditions, surface slope, aspect, and other extraneous factors (Lillesand *et al.*, 2007). Performance issues arise by forest masks based on NDVI because of near infrared band (Hung *et al.*, 2012). The advantage of very high resolution imagery in panchromatic and multi spectral bands will offer exceptional geolocation accuracy, unprecedented precise views for mapping and image analysis. Extraction of NDVI from multispectral data, red and near infrared bands combination has done for accurate detection of

crown sizes and shapes. The spectral signature of vegetation selected from the sunlit side of the tree crown (Bai *et al.*, 2005). Multispectral bands widely used for distinct detection and differentiation of vegetation and improve the spectral discrimination of rock/soils in the VNIR (VIS/NIR) range. In this study, band 3 and 4 of GeoEye-2 were representing the red and near infrared bands. Figure 15 shows the NDVI image of the study location.

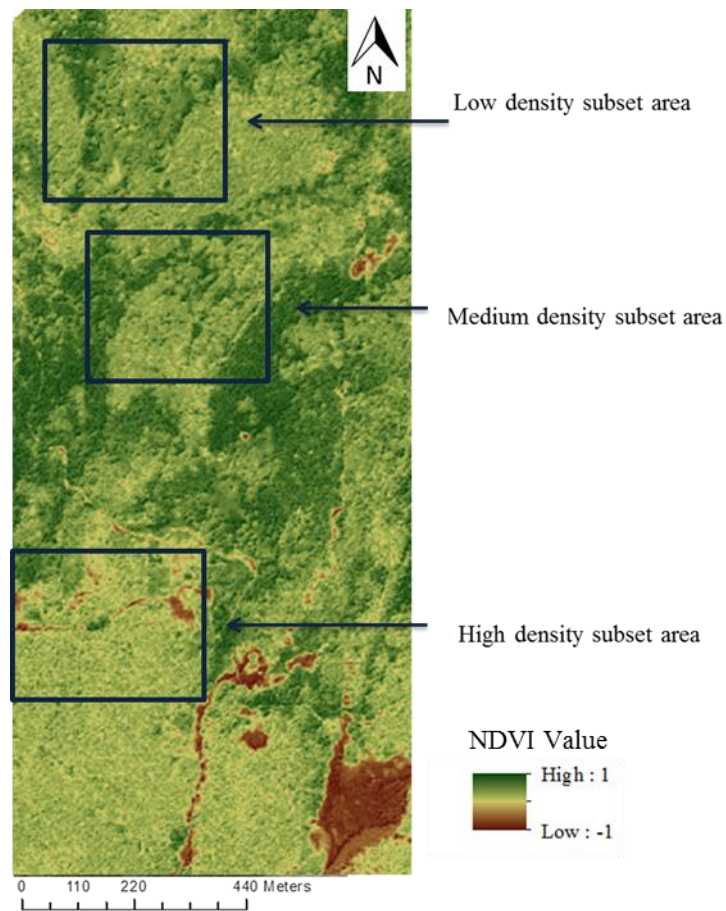


Figure 15, Normalized Difference Vegetation Index (NDVI) layer of the study area and the location of subset areas for June 2012.

Individual Tree Top Detection and Crown delineation by Marker-Controlled Watershed algorithm

Individual tree detection, in this study, refers to the procedure of identifying individual tree locations by tree tops and their respective crown segments. Tree top identification is particularly a primary step

towards individual crown isolation (Persson *et al.*, 2002; Pouliot *et al.*, 2002; Kim *et al.*, 2010) especially by using an image segmentation approach. Detection of individual tree tops also provides the advantage of better precision in the prediction of many forest variables (Ke and Quackenbush, 2011). Various individual tree detection methods have already been reviewed in this study's Chapter 1.

In the image with average brightness the brightest pixels present tree top points. However, the brightest pixel of the crown is not necessarily the geometric top of it (Novoty *et al.*, 2011). This pixel selection depends on the actual sun angle and sensor angle configuration. The first order Edge detection operations are Roberts, Sobel and Perwitt. The Laplacian could be second order and the main disadvantage of it, is to respond very strongly to noise. Gaussian operations with different standard deviations as a low pass filter can be used to smooth the image and edge detection (Jain, 1989). In this study the local maximum filtering was chosen to detect tree tops because the method mainly could be applied to both datasets hence a good basis for comparison. This step added inside the Marker-Controlled Watershed segmentation algorithm. The approach assumes that regardless to the differences in measurement units, the local maximum pixel brightness value in both datasets represents the peak (Wulder *et al.*, 2000; Pouliot *et al.*, 2002).

The behaviour of four segmentation schemes (i.e., multispectral, LiDAR and multispectral, LiDAR, NDVI based) examined by using Marker-Controlled Watershed algorithm. We hypothesized that there is a complementarity in the two data sources that will help in tree crown delineation accuracy by having the NDVI as ancillary data. The CHM and multispectral band derived from the both data sets and used as additional features in the object-based segmentation approach. Marker-Controlled Watershed algorithm with morphological techniques as explained in Chapter 1 is going to be evaluated during the research. The purpose of using morphological techniques was to reduce the artefacts of CHM and multispectral data, because of the gaps in canopy cover which called pits.

In Marker-Controlled Watershed algorithm a grey-level image may be seen as a topographic relief, where the grey level of a pixel is interpreted as its altitude in the relief (Figure 16). A drop of water falling on a topographic relief flows along a path and finally reaches to a local minimum (Dong and Li, 2011). The steps of the presented Marker-Controlled Watershed algorithm in Matlab © are described in the following bullets and Figure 19.

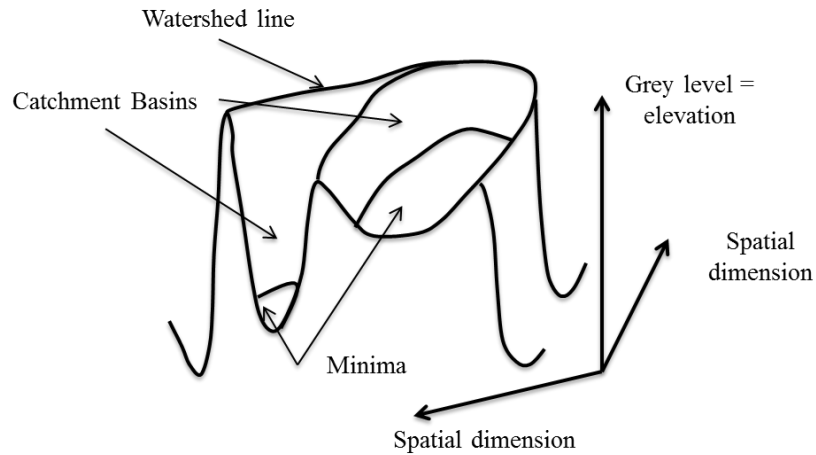


Figure 16, Watershed segmentation grey level profile of image data, local minima of grey level yield catchment basins, local maxima define the Watershed lines (Tarabalka *et al.*, 2010).

- First step is to read an image and then convert it to a grey level image.
- Second step is to run Sobel filter in 2 directions as edge detection filter (Figure 17)

$$S(x, y) = \sqrt{(D_x(x, y))^2 + (D_y(x, y))^2} \quad \text{Equation 1}$$

-1	0	+1
-2	0	+2
-1	0	+1

x filter

+1	+2	+1
0	0	0
-1	-2	-1

y filter

Figure 17, The 3 by 3 kernel of Sobel filter (edge detection) in 2 directions.

- Third step is to compute the foreground markers by opening and closing reconstruction from morphological techniques to not missing the small trees.

- Forth step is computing the background markers for identifying crown areas by morphological distance transformers (Figure 18).
- Fifth step is modifying the segmentation function to avoid disturbance of background.

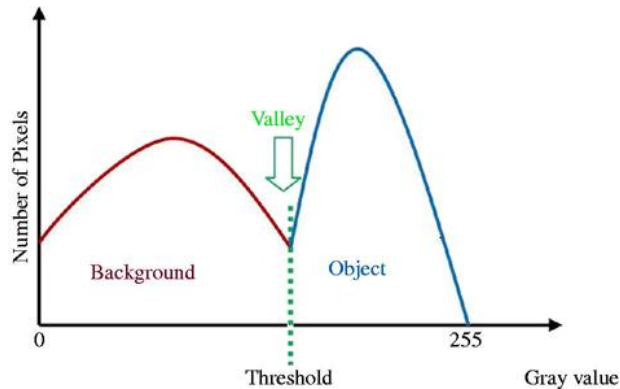


Figure 18, Morphological techniques, erosion and dilation for the back ground markers (Adapted from Ted Wu, 1999).

- Sixth step is the computation of Watershed transform.
- Seventh step is a visualization of the tree top markers, background markers and crown delineation on the original image.

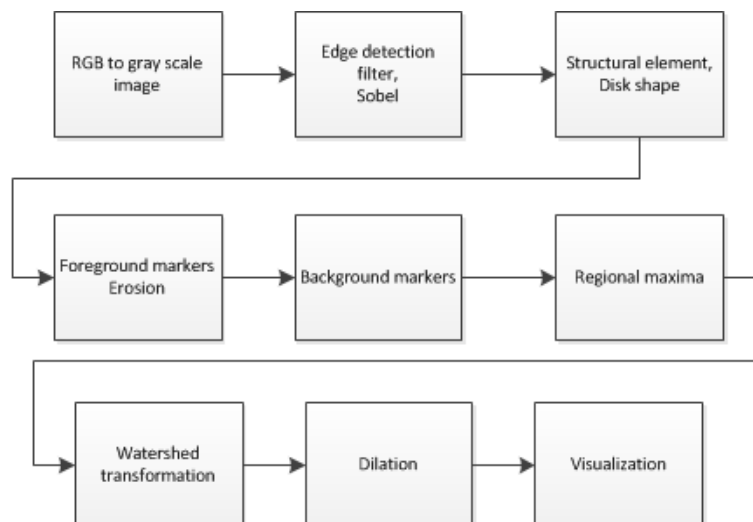


Figure 19, Steps of Marker-Controlled Watershed segmentation algorithm with morphological techniques.

The provided Marker-Controlled Watershed algorithm defined with four main thresholds based on the data which had been collected in 2012 field work (Ruparelia, 2012). These thresholds are 1) Strel threshold (Structuring Element) , this function in Matlab marked the foreground markers by morphological techniques, opening as an erosion then followed by a dilation, based on the shape & parameter (Kim, 1998) of the average individual tree crown collected in the study area; 2) Dimensional connectivity, calculation of the regional maxima to obtain good foreground markers; 3) Threshold to remove from a binary image all connected components (objects) that have fewer than P pixels which is the smallest crown size in the area (0.5 meter); 4) Image conversion to a binary image threshold, used by Otsu's method (Wang and Dong, 2007), a normalized intensity value that lied in the range of [0, 1] (Zhang and Hu, 2008).

Individual tree top detection and crown delineation Accuracy assessment

The tree top detection and crown delineation were tested and the error of each could be assessed independently on an individual tree basis and for aggregated data. Clinton *et al.*, (2010) summarized different segmentation accuracy assessments which have been used by many researchers. They introduced over-segmentation and under-segmentation as accuracy assessment of the segmented image. The maximum diameter of each tree crown had measured along the east-west direction because of the south to north shadow direction and to avoid measurement outliers (Pouliot *et al.*, 2002; Bai *et al.*, 2005).

Tree detection accuracy has been well researched and is commonly performed at an individual tree level using reference data consisting of trees locations visually interpreted from the imagery or from field data (Brandtberg and Walter, 1998; Gougeon, 1995; Heinzl *et al.*, 2008). However, the number of missed and wrong identified trees cannot be evaluated for algorithm testing (King *et al.*, 2002). Tree delineation accuracy has not commonly been evaluated because of the difficulty of precisely measuring tree crowns in the field. Field-based crown measurements are containing errors relating to how well field personnel can project the crown boundary to a measuring device and identification of a suitable boundary to measure the tight overlap or irregular crowns. Studies in forests have commonly used crown diameter from visual interpretation to evaluate delineation accuracy (Ghosh *et al.*, 2014). For detection and delineation accuracy purpose, comparing a truth map based on the prior knowledge of tree locations (fieldwork 2012) and detected top is available (Ke *et al.*, 2010). For each known tree, a single detected top within the boundary of crown

was chosen to represent it and the remainder, if not, then they were counted as commission errors (Pouliot *et al.*, 2002). Omission errors were counted when no top detection exists within the boundary of a known crown (Vastaranta *et al.*, 2012).

Each automatically-detected and delineated individual tree were lying within one of the following categories based on the photogrammetrically or terrestrial measured tree plots (Koch *et al.*, 2006). Crown delineation accuracy assessment in this study based on how well each delineated crown as segment matched with the ground reference delineation. These reference crowns digitized manually from the field data crowns in Arc GIS ©. Leckie *et al.*, (2003) stated that a "Perfect" match with a ground reference field data is declared when one to one correspondence achievable between segments and crowns and their respective overlaps more than 50%. Other groups as "Good" match related to one to one correspondence but the individual crown is too big where there might be several individual crowns associated by minor overlap with each other. Third group as "Split", where there are several crowns within a big one without belonging to ground reference crown delineation and not belong to two before mentioned groups (Figure 20). The accuracy assessment of this study followed the mentioned groups.

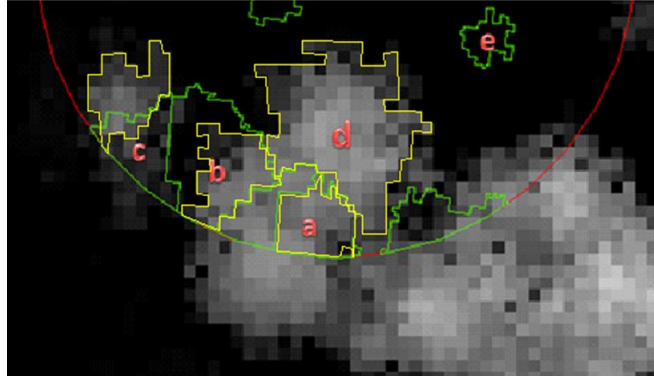


Figure 20, a) Perfect match, b) Good match, c) Split d) Omission and e) Commission. Yellow polygons are ground reference crowns and green polygons are segmentation algorithm results.

One of the nonparametric statistical analysing methods is Chi-square (χ^2) test and often used where the data consist frequencies. This test can be applied to only discrete data which is one the limitations of this test. Chi-square test tells us whether the classifications on a given population are dependent from each other or not. However, it is

important to emphasize that the establishment of statistical association by means of chi-square necessarily does not imply any relationship between the being compared attributes, but it does indicate that the reason for the association is worth investigating. In the Equation 2, O_i stands for observed frequencies, E_i stands for expected frequencies and n indicates the number of cells or frequencies.

$$\chi^2 = \sum_{i=1}^n \frac{(O_i - E_i)^2}{E_i} \quad \text{Equation 2}$$

The main idea behind chi-square specification tests is to test the significance of results and to measure the 'distance' between the empirical cell frequencies and their model-based (Plackett, 1900; MaCurdy and Ryu, 2003). This test allows comparing a collection of categorical data with some theoretical expected distribution which be matched segments and omission ones in this study. A chi-square (χ^2) statistic is used to investigate whether distributions of categorical variables differ from each other (Hauschild and Jentschel, 2001). We want to determine whether the accurate segmentation of individual crowns based on the combination of multispectral imagery and LiDAR data is dependent on NDVI contribution in the algorithm. By statistical convention, we use the 0.05 probability level as our critical value (Canal, 2005). If the calculated chi-square value is less than the 0.05 value, we accept the hypothesis. If the value is greater than 0.05, we reject the hypothesis of this study. Consequently, chi-square test, if properly applied may give us the answer by rejecting the null hypothesis.

Chapter 3

3.1 Results

For three subset area, the four schemes of input data combinations were applied. The three subset areas were denoted low, medium and high density, where low density represented the sparse forest category and high density complex canopy cover (Chapter 2). The segmentation results in four schemes: delineation with multispectral (GeoEye-2) imagery, with LiDAR, based on integration of multispectral and LiDAR and finally with contribution of NDVI, of tree crowns per subset area (Figure 21) presented accordingly from Table 4 to Table 7.

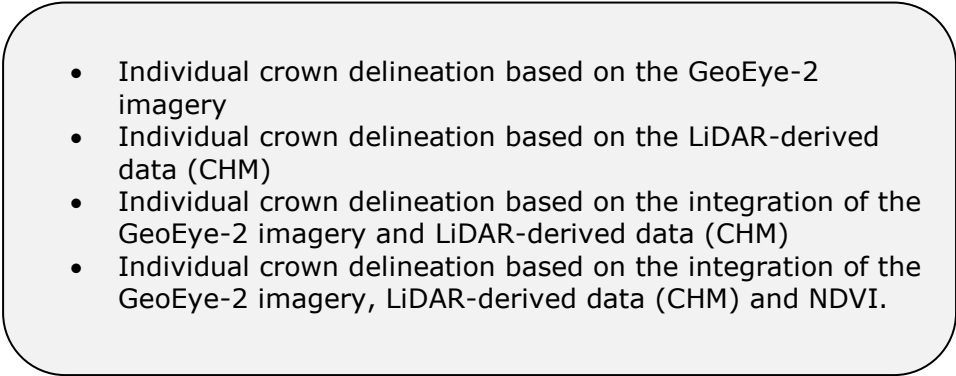
- 
- Individual crown delineation based on the GeoEye-2 imagery
 - Individual crown delineation based on the LiDAR-derived data (CHM)
 - Individual crown delineation based on the integration of the GeoEye-2 imagery and LiDAR-derived data (CHM)
 - Individual crown delineation based on the integration of the GeoEye-2 imagery, LiDAR-derived data (CHM) and NDVI.

Figure 21, Input data methods for extracting individual crowns.

3.1.1 Crown delineation with GeoEye-2 imagery

In general the matching between individual crown delineation by Marker-Controlled Watershed segmentation and the ground reference trees collected in 2012 field work was less than 50% (Table 4). Over all three plots (low, medium and high density), 41.9% of the ground reference delineations had corresponding segments that were considered perfect matches, 24.4 % had good matches and 6.9% as split. From these matches, the segments were generally similar size of the ground reference delineations. The low density subset area plots had the highest accuracy of perfect matches and high density subset the least. Figure 22 provides a summary of the segmentation accuracy results versus ground reference crowns.

Results

Table 4, Correspondence of individual tree crown delineation versus ground reference crowns based on multispectral imagery

Subset area type	Match type			Commission n (%)	Omission n (%)	Total ground crowns
	Perfect n (%)	Good n (%)	Split n (%)			
Low density	43 (39.4)	35 (32.1)	10 (9.1)	7 (6.4)	13 (11.9)	109
Medium density	38 (42.2)	20 (22.2)	8 (8.8)	9 (10)	14 (15.5)	90
High density	46 (44.2)	19 (18.2)	3 (2.8)	12 (11.5)	18 (17.3)	104
Total	127 (41.9)	74 (24.4)	21 (6.9)	28 (9.2)	45 (14.8)	303

Note: (n) refers to number of individual trees as segments and (%) refers to percentage of each category

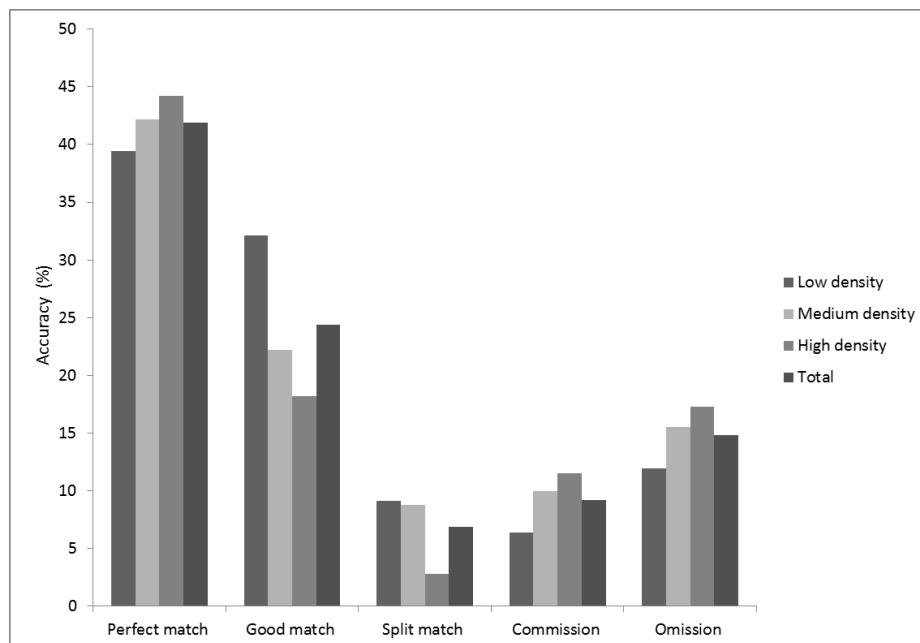


Figure 22, Statistical accuracy histogram of individual tree crown delineation versus ground reference crowns based on multispectral imagery.

Commission error was large for the high density subset area plots (11.5%). There were 7 and 9 commissions for low and medium density, respectively, which was 6.9% and 9.2% of total ground individual crowns in the plots. The ground reflectance from the gaps between trees canopies of the multispectral imagery in the segmentation algorithm lead to the commission delineations (Figure 23). In the definition of Marker-Controlled Watershed algorithm (Chapter 2) one of the main thresholds was focused on any crown segmentation with the size less than 0.5 meter (smallest crown size in the study area) would be rejected as a tree crown segment.

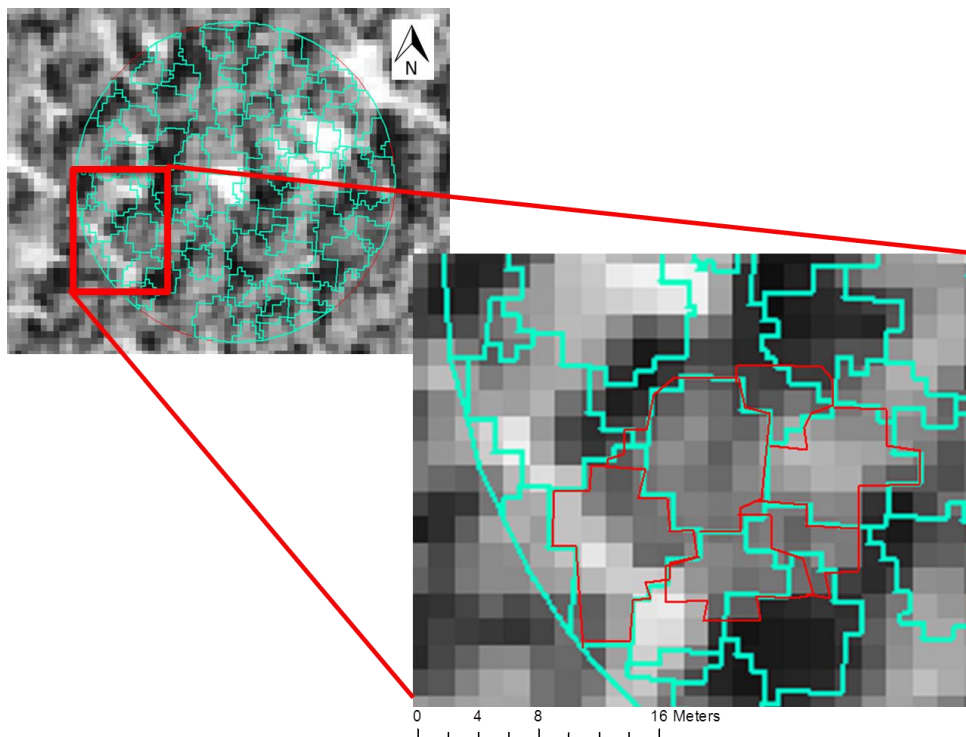


Figure 23, An example of tree crown segmentation for the single plot in the low density subset area. Red polygons are ground reference crowns and cyan polygons are algorithm results.

3.1.2 Crown delineation with LiDAR data

Segmentation of individual tree crowns in the subset areas based on the LiDAR data in total was 20 % more accurate than the multispectral based one (Figure 24). Unlike the multispectral imagery omission segments were not a problem here. There were a higher percentage of perfect matches (60.3%) and more highly represented trees (66.6%) for the medium density subset area. There were 7 cases of omission in the overall of 3 subset areas of crown delineation by LiDAR data. The segments derived from the CHM were often smaller than the ground reference delineation and corresponding multispectral GeoEye-2 imagery. By evaluating all of the segments, 60.3% were considered perfect match, 21.1% were good match, 4.2% as split and 6.6% commissions (Table 5).

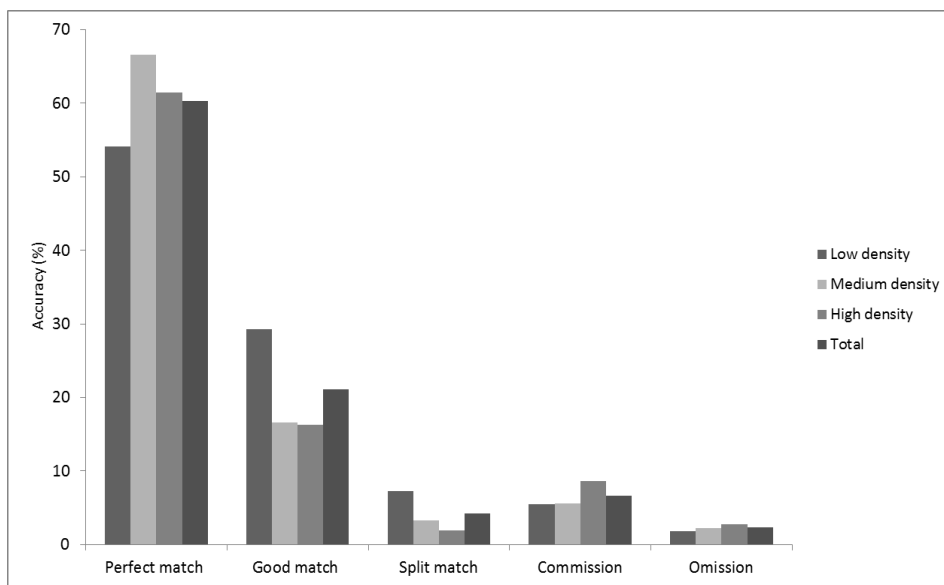


Figure 24, Statistical accuracy histogram of individual tree crown delineation versus ground reference crowns based on LiDAR data.

Table 5, Correspondence of individual tree crown delineation versus ground reference crowns based on LiDAR data

Subset area type	Match type			Commission n (%)	Omission n (%)	Total ground crowns
	Perfect n (%)	Good n (%)	Split n (%)			
Low density	59 (54.1)	32 (29.3)	8 (7.3)	6 (5.50)	2 (1.8)	109
Medium density	60 (66.6)	15 (16.6)	3 (3.3)	5 (5.55)	2 (2.2)	90
High density	64 (61.5)	17 (16.3)	2 (1.9)	9 (8.6)	3 (2.8)	104
Total	183 (60.3)	64 (21.1)	13 (4.2)	20 (6.6)	7 (2.3)	303

Note: (n) refers to number of individual trees as segments and (%) refers to percentage of each category

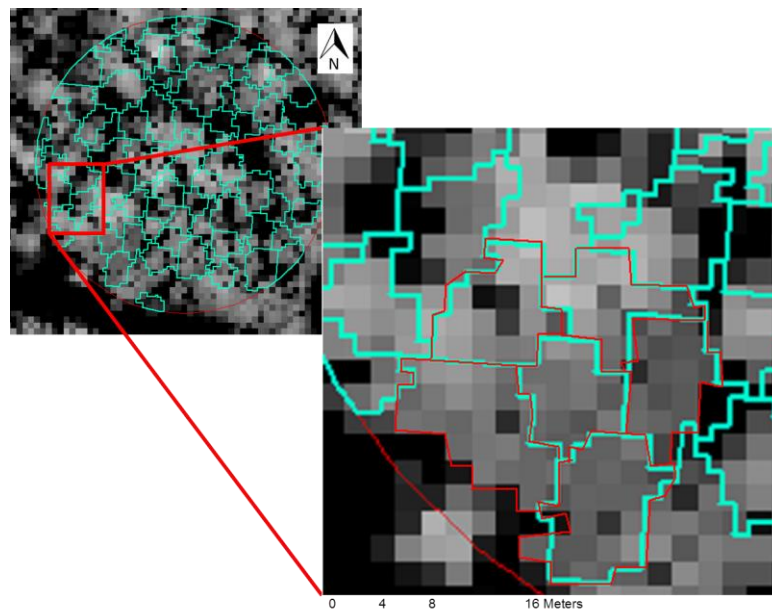


Figure 25, An example of tree crown segmentation for the single plot in the low density subset area. Red polygons are ground reference crowns and cyan polygons are algorithm results.

Using canopy height model (CHM) improved the number of perfect matches for segmentation purpose and reduced the number of commissions and omissions. Figure 24 presents the statistical histogram of accuracy results. Above Figure 25 shows an example plot in the low density subset area with extracted segments from the algorithm based on LiDAR data input.

3.1.3 Crown delineation with integration of GeoEye-2 imagery and LiDAR data

Accuracy assessment of the segments derived from the integration of LiDAR data and multispectral GeoEye-2 imagery validated by ground reference segments presents in Table 6 and Figure 26.

Table 6, Correspondence of individual tree crown delineation versus ground reference crowns for multispectral imagery and LiDAR data integration

Subset area type	Match type			Commission n (%)	Omission n (%)	Total ground crowns
	Perfect n (%)	Good n (%)	Split n (%)			
Low density	62 (56.8)	21 (19.2)	6 (5.5)	5 (4.5)	12 (1.8)	109
Medium density	60 (66.6)	14 (15.5)	2 (2.2)	6 (6.6)	4 (4.4)	90
High density	68 (65.3)	8 (7.6)	3 (2.8)	10 (9.6)	7 (6.7)	104
Total	190 (61.7)	43 (14.4)	11 (3.6)	21 (6.9)	13 (4.2)	303

Note: (n) refers to number of individual trees as segments and (%) refers to percentage of each category

Above table indicates the effectiveness of using integration of multispectral imagery and LiDAR datasets for individual crown delineation. Tree segments determined for each of the ground reference delineations were statistically tested with T-test to the results derived from the CHM. The overall accuracies are: perfect

match 61.7%, 14.4% for good, 6.9% as commissions and 4.2% as omissions. The T- test statistical results presents in Table 7.

Table 7, Summary of statistical test for samples from LiDAR based data segmentation versus GeoEye-2 imagery and LiDAR integration

		Paired Differences					
		Mean	Std. Deviation	Std. Error Mean	95% Confidence Interval of the Difference		t
					Lower	Upper	
Pair 1	SL - L	-3.00000	6.29285	2.56905	-9.60394	3.60394	-1.168

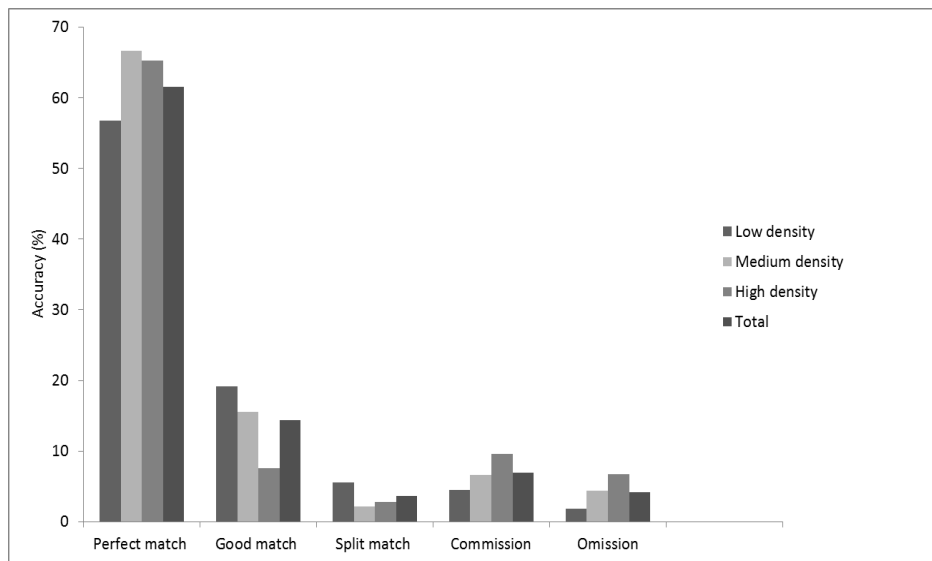


Figure 26, Statistical accuracy histogram of individual tree crown delineation versus ground reference crowns based on the multispectral imagery and LiDAR data integration.

3.1.4 Crown delineation with GeoEye-2 imagery, LiDAR data and NDVI

Those ground reference crowns having the good match type segmentation were 2.6% improved by adding NDVI as an ancillary

Results

data to LiDAR and GeoEye-2 integration. For all match types of crown segmentation, commission ranges from 4.5% in low density till 6.7% in high density (Table 8). Results of matched crown segments by Marker-Controlled Watershed algorithm and NDVI improved to 59.6% for low density and 68.8% for medium density. Figure 27 presents the results of crown delineation by contribution of NDVI to the integration of GeoEye-2 imagery and LiDAR data canopy height model. The green colour polygons defined by segmentation algorithm and the effect of shadows or gaps between canopy surface had been removed in most of the good match type of segments. The crown boundaries defined by containing less shadow part of trees which improve the accuracy of delineation in sparse forest. However, the effect of shadows and gaps more distinguishable in low density subset area in compare with the denser canopy covers of the study area. The statistical evaluation of segmentation results from integration presents in Figure 28.

Table 8, Correspondence of individual tree crown delineation versus ground reference crowns for multispectral imagery, LiDAR data and NDVI integration

Subset area type	Match type			Commission n (%)	Omission n (%)	Total ground crowns
	Perfect n (%)	Good n (%)	Split n (%)			
Low density	65 (59.6)	30 (27.5)	3 (2.7)	5 (4.5)	3 (2.7)	109
Medium density	62 (68.8)	12 (13.3)	1 (1.11)	7 (7.7)	5 (5.5)	90
High density	68 (65.3)	8 (7.6)	3 (2.8)	10 (9.6)	7 (6.7)	104
Total	198 (65.3)	60 (19.8)	7 (2.3)	22 (7.2)	15 (4.9)	303

Note: (n) refers to number of individual trees as segments and (%) refers to percentage of each category

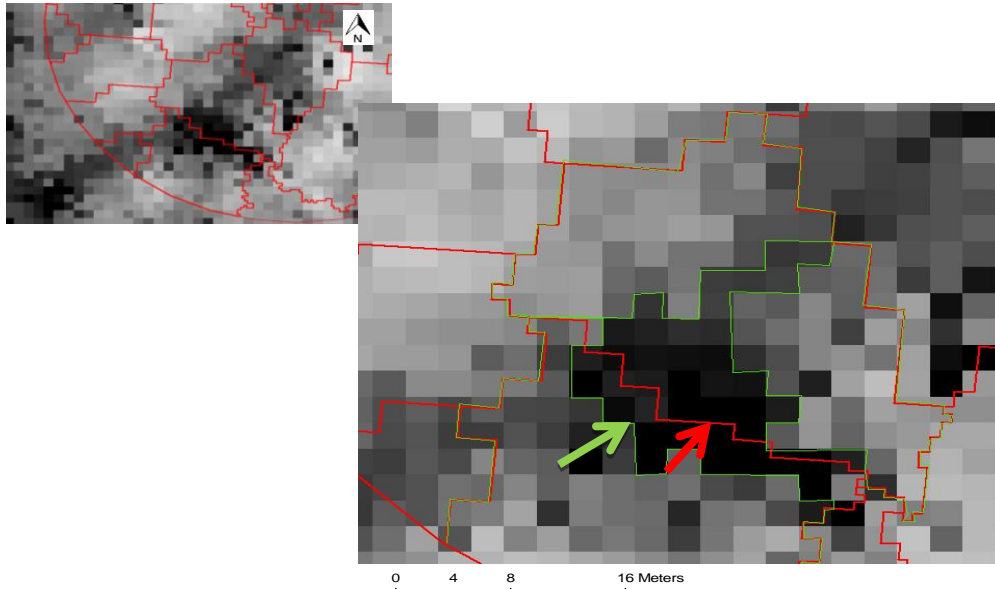


Figure 27, An example of Crown delineation on low density subset area by Marker-Controlled Watershed segmentation on GeoEye-2, CHM and NDVI integration. Red polygons are ground reference crowns and green crowns are segmentation algorithm results.

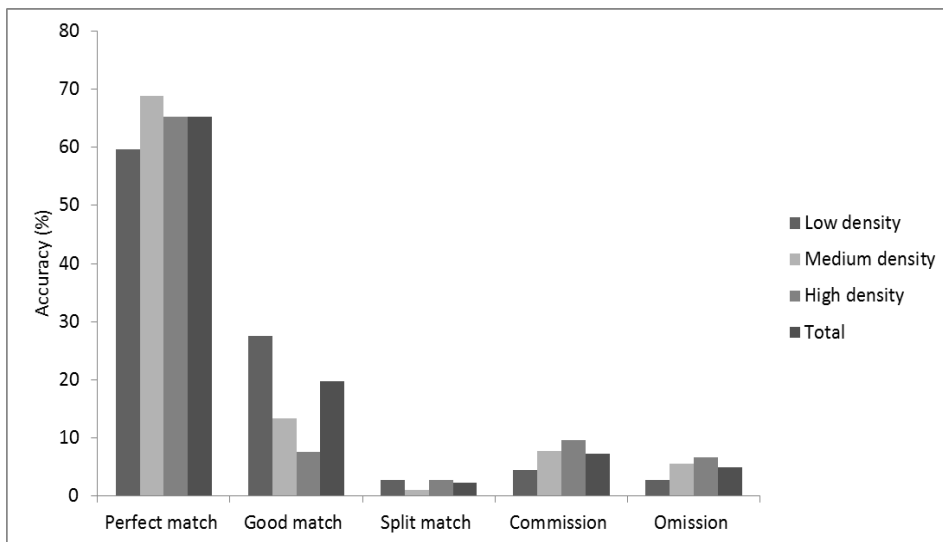


Figure 28, Statistical accuracy histogram of individual tree crown delineation versus ground reference crowns based on the multispectral imagery, LiDAR data and NDVI integration.

3.1.5 Comparison of the four techniques in low, medium and high density canopy covers subset areas

Overlapped crowns in the subset areas tended to be underestimated by delineation algorithm. Using NDVI as an ancillary data improved the results for low density subset plots significantly. Statistics significance reported with degrees of freedom and the Pearson chi-square value (rounded to two decimal places). The significance level for each subset area separately represent in Table 9, Table 10 and Table 11.

Pearson chi-square test result for one degree of freedom in the comparison of GeoEye-2 imagery segmentation and LiDAR for low density was 0.016, while for medium density subset was 0.002. As the result is less than critical value of Alfa 0.73 mentioned in (see Chapter 2), so the improvement in accuracy of object-based segmentation approach had been accepted. However, for the comparison of LiDAR and GeoEye-2 integrated with LiDAR only on the low density subset area by $\chi^2(1,101) = 0.009, p = 0.05$ was accepted. Finally, the percentage of delineated crowns by adding NDVI to the LiDAR and GeoEye-2 combination to the same combination without considering the NDVI for low density subset are was $\chi^2(1,101) = 0.016, p = 0.05$ which presented the significance effect of adding NDVI on crown segmentation by reducing the effect of shadows and gaps.

Table 9, Summary of statistical test for segmentation results of Geoeeye-2 imagery, LiDAR based vs. GeoEye-2 imagery, LiDAR and NDVI based in low density subset area

Chi-Square Tests					
	Value	df	Asymp. Sig. (2-sided)	Exact Sig. (2-sided)	Exact Sig. (1-sided)
Pearson Chi-Square	5.833 ^a	1	.016		
Continuity Correction ^b	4.609	1	.032		
Likelihood Ratio	6.216	1	.013		
Fisher's Exact Test				.029	.014
Linear-by-Linear Association	5.804	1	.016		
N of Valid Cases	202				

a. 0 cells (.0%) have expected count less than 5. The minimum expected count is 7.50.

b. Computed only for a 2x2 table

Table 10, Summary of statistical test for segmentation results of Geoeye-2 imagery, LiDAR based vs. Geoeye-2 imagery, LiDAR and NDVI based in medium density subset area

Chi-Square Tests					
	Value	df	Asymp. Sig. (2-sided)	Exact Sig. (2-sided)	Exact Sig. (1-sided)
Pearson Chi-Square	.118 ^a	1	.732		
Continuity Correction ^b	.000	1	1.000		
Likelihood Ratio	.118	1	.731		
Fisher's Exact Test				1.000	.500
Linear-by-Linear Association	.117	1	.732		
N of Valid Cases	160				

a. 2 cells (50.0%) have expected count less than 5. The minimum expected count is 4.50.
b. Computed only for a 2x2 table

Table 11, Summary of statistical test for segmentation results of Geoeye-2 imagery, LiDAR based vs. Geoeye-2 imagery, LiDAR and NDVI based in high density subset area

Chi-Square Tests					
	Value	df	Asymp. Sig. (2-sided)	Exact Sig. (2-sided)	Exact Sig. (1-sided)
Pearson Chi-Square	.000 ^a	1	1.000		
Continuity Correction ^b	.000	1	1.000		
Likelihood Ratio	.000	1	1.000		
Fisher's Exact Test				1.000	.609
Linear-by-Linear Association	.000	1	1.000		
N of Valid Cases	172				

a. 0 cells (.0%) have expected count less than 5. The minimum expected count is 7.00.
b. Computed only for a 2x2 table

The overall results present for each subset area with four different methods in the following tables and figures. For low density subset area Table 12 and Figure 29, medium density with Table 13 and Figure 30 and high density by Table 14 and Figure 31.

Results

Table 12, Correspondence of individual tree crown delineation versus ground reference crowns for low density subset area

	<i>Match type</i>				
	<i>Perfect (%)</i>	<i>Good (%)</i>	<i>Split (%)</i>	<i>Commission%</i>	<i>Omission%</i>
Multispectral	41.9	24.4	6.9	9.2	14.8
LiDAR	60.3	21.1	4.2	6.6	2.3
Multispectral & LiDAR	61.7	14.4	3.6	6.9	4.2
Multispectral & LiDAR & NDVI	65.3	19.8	2.3	7.2	4.9

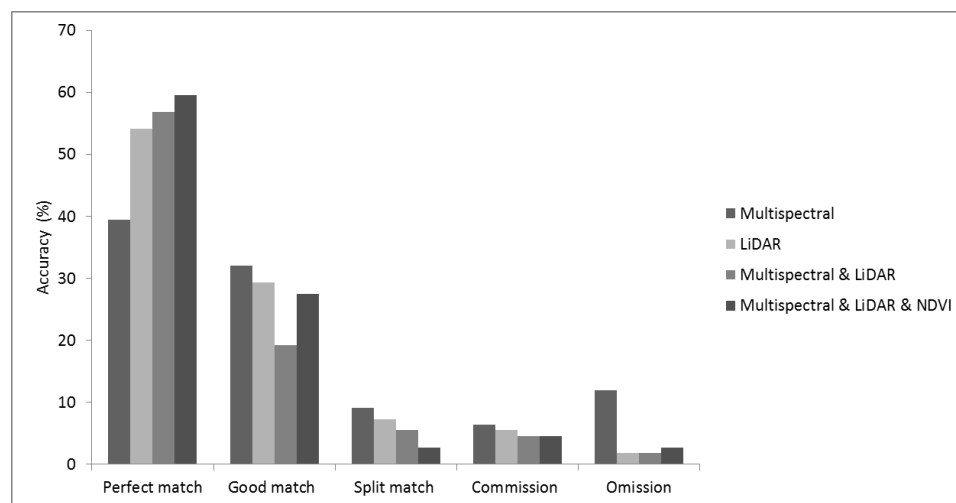


Figure 29, Statistical accuracy histogram of individual tree crown delineation versus ground reference crowns for the low density subset area.

Table 12 provides a summary of the segmentation results of four methods for low density subset area. The best accuracy were achieved for the combination of GeoEye-2 imagery and LiDAR data method with contribution of NDVI. As Figure 29 shows the lowest

result belong to the GeoEye-2 imagery based method also the highest omission segments percentage.

In the case of medium density subset area, the lowest value of accuracy belongs to the GeoEye-2 imagery based method but also the highest accuracy in good match type. This result means to the importance of spectral data in denser canopy surfaces. However, the relatively highest accurate segments in perfect match type still belong to the dataset combined with NDVI (Figure 30).

Table 13, Correspondence of individual tree crown delineation versus ground reference crowns for medium density subset area

	<i>Match type</i>				
	<i>Perfect (%)</i>	<i>Good (%)</i>	<i>Split (%)</i>	<i>Commission%</i>	<i>Omission%</i>
Multispectral	42.2	22.2	8.8	10	15.5
LiDAR	66.6	16.6	3.3	5.55	2.2
Multispectral & LiDAR	66.6	15.5	2.2	6.6	4.4
Multispectral & LiDAR & NDVI	68.8	13.3	1.11	7.7	5.5

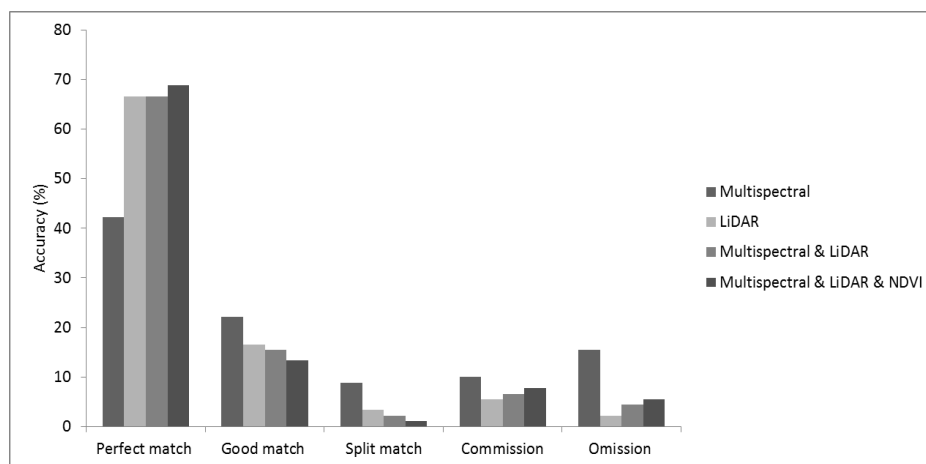


Figure 30, Statistical accuracy histogram of individual tree crown delineation versus ground reference crowns for the medium density subset area.

Results

We further tested the methods for high density subset area as well as the other subset areas for segmentation approach. As expected, the results of both methods are almost the same (Figure 31). The multispectral data based segmentation is still the highest rank recorded for oversegmentation problem even by using the combination of two datasets. In the high density the existing of NDVI did not improve the accuracy results as the shadows are not clear to detect.

Table 14, Correspondence of individual tree crown delineation versus ground reference crowns for high density subset area

	<i>Match type</i>				
	<i>Perfect (%)</i>	<i>Good (%)</i>	<i>Split (%)</i>	<i>Commission%</i>	<i>Omission%</i>
Multispectral	44.2	18.2	2.8	11.5	17.3
LiDAR	61.5	16.3	1.9	8.6	2.8
Multispectral & LiDAR	65.3	7.6	2.8	9.6	6.7
Multispectral & LiDAR & NDVI	65.3	7.6	2.8	9.6	6.7

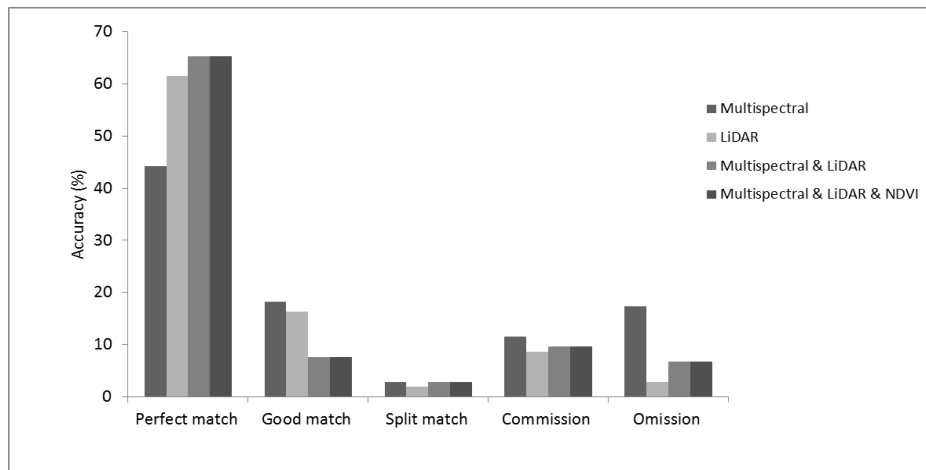


Figure 31, Statistical accuracy histogram of individual tree crown delineation versus ground reference crowns for the high density subset are.

Chapter 4

4.1 Discussion

Novelty of this study is the following: accuracy of crown delineation in sparse forest improved statistically significant by reducing the effect of shadows and within crown gaps. In the previous studies, the ability of ancillary data to support the individual crown delineation results such as topographic information (Hutchinson, 1982; Ricchetti, 2000), spectral-derived texture (Chica-Olmo and Abarca-Hernandez, 2000; Li and Eastman, 2006) and radar-derived texture (Mather *et al.*, 1998; Dong and Leblon, 2004) have assessed. Although these approaches are quite useful, they are also time consuming and considered as highly subjective delineation processes (Skidmore, 1989; Franklin, 2001). Consequently, using digital remotely sensed data and image segmentation techniques have been advanced to assist in forest inventories with more objective aspects than subjective (Pascual *et al.*, 2008). Therefore in this study we tested four schemes for accurate crown delineation approach and obtained results (Chapter 3) that were slightly better with the latter approach, especially for objects with poor contrast. While the last method would provide the better definition of the object homogeneity, it increases the time of processing with the number of layers because each layer must be individually segmented.

The NDVI of multispectral imagery based on spectral and spatial resolution (Bhandari *et al.*, 2012) was used in this study as ancillary data. Variation in reflectance of canopy surface in forestry across different spectral band provides a fundamental mechanism for understanding the objects in remotely sensed image (Jackson and Huete, 1991). This potential of the NDVI assessed the quality of segmentation to identify the crowns from backgrounds more accurately. Identification of objects is greatly dependent on the multispectral optical imagery and LiDAR data integration resolution. At fine resolution image, e.g. 15 cm resolution of rasterized LiDAR data, it guarantees the recognition of less than a single crown. However, its application at lower spatial resolution such as our available satellite image data (50 cm resolution) produced errors. As a result, spectral differences between shadows and crowns generated systematic segmentation of individual crowns in 50 cm resolution (Drăguț *et al.*, 2014). From this perspective, NDVI performed well in low density canopy cover in compare with denser areas. However,

the most important indicator of the segmentation algorithm for accuracy of the delineated crowns is structuring element.

The Structuring Element of Marker-Controlled Watershed algorithm blurs between crown valleys in the original grey scale image and leads to coarse segment boundaries which may be misaligned by the within crown gaps. In addition, Structuring Element has a regular defined disk shape for crown shapes but in reality most of the individual tree crowns have irregular shapes. Adapting the structural element threshold to perform accurate segmentation resulted in the challenge of specifying and calculation of the average crown size kernel. For example at a fine resolution of LiDAR derived CHM all branches in a tree crown are visible thus the smallest crowns are detectable by kernel. However, in a coarser resolution, here GeoEye-2 and CHM with 0.5 meter, a single tree crown merges with its neighbours, thus introducing error in segmentation or recognition process. This kernel makes the algorithm dependent to the specific sensor resolution, forest type and the integration of multiple datasets such as ancillary data. Higher omission errors in delineation results refer to the fixed structuring element kernel size in Marker-Control Watershed algorithm based on the mean crown radius from fieldwork for defining tree top and crown boundary. Thus the mentioned kernel is not suitable for very small crowns as well as very large crowns which make high omission and commission errors, respectively (Pouliot *et al.*, 2002). Later, 3D segmentation algorithms tried to separate individual trees, minimizing the similarities between the segments and maximizing those within segments (Reitberger *et al.*, 2009).

Integration of GeoEye-2 imagery, LiDAR and ancillary data (here NDVI) has been found important in the segmentation algorithms for tree top detection and crown delineation. Leckie *et al.*, (2003) found the combination of very high resolution multispectral imagery and high density point cloud LiDAR data for individual crown analysis, offers large potentials. The individual crown delineation methods for imagery is mostly perform at a single spatial resolution, typically at the original resolution at which the imagery was acquired (Wang and Xu, 2010). These methods normally require reference points, such as tree tops, for image segmentation (Jing *et al.*, 2012). As mentioned in Chapter 1 and following Chapter 2, the accuracy of tree top detection affects the accuracy of crown delineation which is the primary step in the segmentation algorithm. However, we noted that a fixed structuring element kernel size for regional maxima function in the algorithm based on mean crown radius provides an alternative to estimate tree positions. Khosravipour *et al.*, (2013) implemented a

new algorithm for generating a pit-free CHM from different LiDAR point cloud densities to improve the accuracy of individual tree top detection. As those filtering methods do not accurately remove the LiDAR noises (pits) but alter all pixels of canopy surface which in result affects the original structure of tree crown. Segmentation of the individual tree of this study is less accurately matched with the ground reference crowns; in the case of low density subset are based on multispectral data only 41.9 % of the ground reference crowns had perfect matches with the segmented ones. Results were even less accurate in the case of denser subset area plots and the error measurement increased slightly with density.

In this study, results based on LiDAR data and the application of the Marker-Controlled Watershed segmentation technique to high density point cloud data are not presenting the optimum solution for commission and omission errors in the delineation process. Nevertheless, by comparing the results with ground reference crowns from plots reasonable corresponds achieved (60.3% in total for all three subset areas had perfect matches with ground references). Accuracy was higher for high density subset area (61.5% for perfect match) in comparison with 44.2% for the same subset area in the GeoEye-2 imagery based scheme. There were fewer split trees on the LiDAR based tree crown segments, but it is not necessary concluding that LiDAR data will reduce the number of splitting larger tree segments. The results of accuracy assessment might look poor especially for the multispectral data based method. Certainly the computed accuracy metrics depend on the reference data. In this research, reference data comes from the data collection of study area in 2012. The ground reference polygons as segments were manually mapped. However, visual interpretation with the reference data mapping for validation purposes increased the errors in the segmentation accuracy.

Chapter 5

5.1 Conclusions and recommendations

5.1.1 Conclusions

A solution for more accurate individual crown delineation on remote sensing data was missing in object-based segmentation algorithms. We introduced a methodology by adding NDVI for the correct selection of crown boundaries at three different subset areas. Tests on integration of GeoEye-2 imagery and LiDAR data provided statistically satisfactory results in spars forest (Chapter 4).

This research has emphasized the potentials of new remotely sensed data such as high density point cloud LiDAR data and very high resolution multispectral imagery and a combination of both. It concluded that they are suitable for individual tree top detection and crown delineation. There is a strong synergy among the two data sources evaluated in this study. We have tested four individual crown delineation schemes which are: VHR multispectral GeoEye-2 satellite image, High density point cloud airborne LiDAR data, a combination of both LiDAR and multispectral, and a combination of LiDAR and NDVI of the multispectral data. The accuracy of all 4 techniques applied to 3 different subsets of low, medium and high density was assessed using commission and omission error method. As an example, the LiDAR could eliminate most of the omission errors that often happen in open canopies with multispectral remote sensing imagery. However, this optical data produced better crown segmentation results in more dense plots. The Marker-Controlled Watershed segmentation approach by its fundamentals of morphological techniques should deal with the considered over-segmentation problem with multispectral data as well as LiDAR data.

The concept of combining very high resolution imagery and high point density LiDAR data for individual tree crown delineation analysis has been tested, presented and a demonstration conducted. For the three subset areas in the Bois noir forest with varying densities, the combination of two datasets with ancillary data gave reasonable accuracy of tree segmentation. The NDVI contribution improves the accuracy of crown delineation significantly in low density subset area and decrease the effect of shadows and gaps. This study presents a test in a specific forest condition and further testing in different forest conditions is necessary. A series of researches, development challenges, operational and cost issues have to be resolved. However,

the results of this study show that the techniques and used data are important forest inventory purposes tools.

5.1.2 Recommendations

1. In this study further investigation of field methods will be required so as to evaluate the effect of human error and image resolution on the accuracy of the data collected.
2. Further investigation on algorithm thresholds definition, especially on structuring element to identify tree tops and delineated crowns on both LiDAR CHM and the multispectral GeoEye-2 imagery. This strategy may reduce the commission and omission errors in tree detection and delineation.
3. Further investigation on other segmentation methods such as pattern recognition and neural network methods would be useful in individual tree crown analysis. Semi-automatic and full automatic approach for tree top detection and crown delineation in forestry could be tested by these methods.
4. Further investigation on reduce the noise of CHM by Pit-free algorithm on improving the quality of the CHM for tree top detection and crown delineation requires further studies.
5. Further investigation on spatial resolution of data in datasets, multispectral imagery and LiDAR CHM required. This resolution should be suitable for the smallest size of tree crown in the study area.
6. The accuracy of LiDAR height metrics versus field based estimates in mountainous terrain requires further investigation.
7. Accuracy assessment for object-based strategies need further investigation especially methods related to LiDAR as object-based approaches. Most of the methods are statistically pixel-based and not suitable for object-based image analysis purposes.
8. Further investigation on other indices to improve the accuracy of segmentation requires. Indices such as RVI (ratio vegetation index), SAVI (soil-adjusted vegetation index), PVI (Perpendicular Vegetation Index), PR (Biomass estimation index) and etc. to reduce the shadow, gap and branch effects in forest canopies.

References

- Abudal-Rahman, A., Zlatanova, S., & Coors, V. (2006). *Innovations in 3D Geo Information Systems*, 50-67. Berlin, Springer, ISBN 978-3-540-36998-1
- Amiri, N. (2013). Evaluation of different change detection techniques in forestry for improvement of spatial objects extraction algorithms by very high resolution remote sensing digital imagery. *International Archives of the Photogrammetry, Remote Sensing and Spatial Information Sciences, XL-1/W3*, 43-47. doi: 10.5194/isprsarchives-XL-1-W3-43-2013
- Ashraf, M. A., Maah, M. J., & Yusoff, I. (2011). *Introduction to Remote Sensing of Biomass, Biomass and Remote Sensing of Biomass, Dr. Islam Atazadeh (Ed.)*, ISBN: 978-953-307-490-0, InTech, Available from: <http://www.intechopen.com/books/biomass-and-remote-sensing-of-biomass/introduction-to-remote-sensing-of-biomass>
- Bai, Y., Walsworth, N., Roddan, B., Hill, D. A., Broersma, K., & Thompson, D. (2005). Quantifying tree cover in the forest-grassland ecotone of British Columbia using crown delineation and pattern detection. *Forest Ecology and Management*, 212(1-3), 92-100. doi: 10.1016/j.foreco.2005.03.005
- Beck, P. S. A., Atzberger, C., Høgda, K. A., Johansen, B., & Skidmore, A. K. (2006). Improved monitoring of vegetation dynamics at very high latitudes: A new method using MODIS NDVI. *Remote Sensing of Environment*, 100(3), 321-334. doi: <http://dx.doi.org/10.1016/j.rse.2005.10.021>
- Beucher, S. (1990). The watershed transformstion applied to image segmentation. *Centre de Morphologie Mathématique*. Paris. Retrieved on October 2013 from [www .cs.tut.fi /~selinum/ .../pfefferkorn.pdf](http://www.cs.tut.fi/~selinum/.../pfefferkorn.pdf)
- Beuning, L. L., Bowen, J. H., Persson, H. A., Barraclough, D., Bulley, S., & MacRae, E. A. (2004). Characterisation of Mald 1-related genes in *Malus*. *Plant Molecular Biology*, 55(3), 369-388. doi: DOI 10.1007/s11103-004-0904-9
- Bhandari, A. K., Kumar, A., & Singh, G. K. (2012). Feature extraction using Normalized Difference Vegetation Index (NDVI): A Case Study of Jabalpur City. *Procedia Technology*, 6(0), 612-621. doi: <http://dx.doi.org/10.1016/j.protcy.2012.10.074>
- Blaschke, T. (2010). Object based image analysis for remote sensing. *International Journal of Photogrammetry and Remote Sensing (ISPRS)*, 65(1), 2-16. doi: <http://dx.doi.org/10.1016/j.isprsjprs.2009.06.004>

References

- Brandtberg, T., & Walter, F. (1998). Automated delineation of individual tree crowns in high spatial resolution aerial images by multiple-scale analysis. *Machine vision and Applications*, 11(2), pp 64-73. doi:10.1007/s001380050091
- Brandtberg, T., Warner, T. A., Landenberger, R. E., & McGraw, J. B. (2003). Detection and analysis of individual leaf-off tree crowns in small footprint, high sampling density lidar data from the eastern deciduous forest in North America. *Remote Sensing of Environment*, 85(3), 290-303. doi: [http://dx.doi.org/10.1016/S0034-4257\(03\)00008-7](http://dx.doi.org/10.1016/S0034-4257(03)00008-7)
- Brenning, A. (2009). Benchmarking classifiers to optimally integrate terrain analysis and multispectral remote sensing in automatic rock glacier detection. *Remote Sensing of Environment*, 113(1), 239-247. doi: DOI 10.1016/j.rse.2008.09.005
- Brown, E. A., Jansen, R. W., & Lemon, S. M. (1989). Characterization of a Simian Hepatitis-a Virus (Hav) - Antigenic and Genetic Comparison with Human Hav. *Journal of Virology*, 63(11), 4932-4937. doi:0022-538X/89/114932-06502-00/0
- Canal, L. (2005). A normal approximation for the chi-square distribution. *Computational Statistics & Data Analysis*, 48(4), 803-808. doi: <http://dx.doi.org/10.1016/j.csda.2004.04.001>
- Chavez, P. S., Sides, S. C., & Anderson, A. A. (1991). Comparison of three different methods to merge multiresolution and multispectral Data: Landsat TM Spot Panchromatic. *Photogrammetric Engineering & Remote Sensing*, 57(3), 205-303. doi: Doi 0099-1112/91/5703-295\$03.00/0
- Chen, Q., Baldocchi, D., Gong P., & Kelly, M. (2006). Isolating Individual Trees in a Savanna Woodland Using Small Footprint Lidar Data. *Photogrammetric Engineering and Remote Sensing*, 72(8), 923-932. doi: Doi 0099-1112/06/7208-0923/\$3.00/0
- Chica-Olmo, M., & Abarca-Hernandez, F. (2000). Computing geostatistical image texture for remotely sensed data classification. *Computers & Geosciences*, 26(4), 373-383. doi: Doi 10.1016/S0098-3004(99)00118-1
- Clinton, N., Holt, A., Scarborough, J., Yan, L., & Gong, P. (2010). Accuracy assessment measures for object-based image segmentation goodness. *Photogrammetric Engineering and Remote Sensing*, 76(3), 289-299.
- Culvenor, D., Coops, N., Preston, R., & Tolhurst, K. G. (1998). A spatial clustering approach to automated tree crown delineation. Natural Resources, Canadian Forest Service, Canada. 67-80. Retrieved on November 2013 from <http://canopy.evergreen.edu/bcd/content/Citations/Citation.aspx?refid=3266>.

- Desclee, B., Bogaert, P., & Defourny, P. (2006). Forest change detection by statistical object-based method. *Remote Sensing of Environment*, 102(1-2), 1-11. doi: 10.1016/j.rse.2006.01.013
- Dong, P., & Leblon, B. (2004). Rock unit discrimination on Landsat TM, SIR-C and Radarsat images using spectral and textural information. *International Journal of Remote Sensing*, 25(18), 3745-3768. doi: Doi 10.1080/01431160310001632675
- Dong, G., & Li, Z. (2011). The Study of Improved Marker-Controlled Watershed Crown Segmentation Algorithm. *Computer society(IEE)*, 1576-1579. doi: DOI 10.1109/CIS.2011.353
- Dorren, L. K. A., Maier, B., & Seijmonsbergen, A. C. (2003). Improved Landsat-based forest mapping in steep mountainous terrain using object-based classification. *Forest Ecology and Management*, 183(1-3), 31-46. doi: Doi 10.1016/S0378-1127(03)00113-0
- Drăguț, L., Csillik, O., Eisank, C., & Tiede, D. (2014). Automated parameterisation for multi-scale image segmentation on multiple layers. *International Journal of Photogrammetry and Remote Sensing (ISPRS)*, 88(0), 119-127. doi: <http://dx.doi.org/10.1016/j.isprsjprs.2013.11.018>
- Flageollet, J. C., Maquaire, O. , Martin, B. , & Weber, D. (1999). Landslides and climatic conditions in the Barcelonnette and Vars basins (Southern French Alps, France). *Geomorphology*, 30, 65-78. doi: Doi S0169-555X9900045-8
- Flanders, D., Hall-Beyer, M., & Pereverzoff, J. (2003). Preliminary evaluation of eCognition object-based software for cut block delineation and feature extraction. *Canadian Journal of Remote Sensing*, 29(4), 441-452.
- Franklin, E. (2001). *Remote sensing for sustaniable forest management* (1st ed.). CRC Press, ISBN-10: 1566703948
- Ghosh, A., Fassnacht, F. E., Joshi, P. K., & Koch, B. (2014). A framework for mapping tree species combining hyperspectral and LiDAR data: Role of selected classifiers and sensor across three spatial scales. *International Journal of Applied Earth Observation and Geoinformation*, 26(0), 49-63. doi: <http://dx.doi.org/10.1016/j.jag.2013.05.017>
- Gonzalez, R. C., & Woods, R. E. (2007). *Digital Image Processing: Prentice Hall PTR (3rd ed.)*. Prentice Hall, ISBN-10: 013168728X
- Goodwin, N. R., Coops, N. C., & Culvenor, D. S. (2007). Development of a simulation model to predict LiDAR interception in forested environments. *Remote Sensing of Environment*, 111(4), 481-492. doi: DOI 10.1016/j.rse.2007.04.001

References

- Gougeon, F. A. (1995). A Crown-Following approach to the automatic delineation of Individual tree crowns in high spatial resolution aerial images. *Canadian Journal of Remote Sensing*, 21(3), 274-284.
- Gougeon, F. A. (1998). Automatic individual tree crown delineation using a valley-following algorithm and a rule based system. *International forum: automated interpretation of high spatial resolution digital imagery for forestry, Proceedings: Symposium*, 11-23. Natural Resources Canada, Canadian Forest Service, Pacific Forestry Centre, Victoria, BC.
- Gougeon, F. A. (2003). The Individual Tree Crown (ITC) Approach to Forest Inventories: Satellite and Aerial Sensor Considerations. *International Union of Forest Research Organisations (IUFRO)*, 4. Retrieved from <http://cfs.nrcan.gc.ca/publications?id=29604>
- Gougeon, F. A., & Leckie, D. (2006). The Individual Tree Crown Approach Applied to Ikonos Images of a Coniferous Plantation Area. *Photogrammetric Engineering & Remote Sensing*, 72(11), 1287-1297.
- Grebby, S., Naden, J., Cunningham, D., & Tansey, K. (2011). Integrating airborne multispectral imagery and airborne LiDAR data for enhanced lithological mapping in vegetated terrain. *Remote Sensing of Environment*, 115(1), 214-226. doi: <http://dx.doi.org/10.1016/j.rse.2010.08.019>
- Gutman, G. G. (1991). Vegetation indices from AVHRR: An update and future prospects. *Remote Sensing of Environment*, 35(2-3), 121-136. doi: [http://dx.doi.org/10.1016/0034-4257\(91\)90005-Q](http://dx.doi.org/10.1016/0034-4257(91)90005-Q)
- Habib, A. F., Al-Durgham, M., Kersting, A. P., & Quackenbush, P. (2008). Error budget of LiDAR systems and quality control of the derived point cloud. *The International Archives of the Photogrammetry, Remote Sensing and Spatial Information Sciences*, XXXVI(B1), 203-210.
- Hauschild, T., & Jentschel, M. (2001). Comparison of maximum likelihood estimation and chi-square statistics applied to counting experiments. *Nuclear Instruments and Methods in Physics Research Section A: Accelerators, Spectrometers, Detectors and Associated Equipment*, 457(1-2), 384-401. doi: [http://dx.doi.org/10.1016/S0168-9002\(00\)00756-7](http://dx.doi.org/10.1016/S0168-9002(00)00756-7)
- Heinzel, J. N., Weinacker, H., & Koch, B. (2008). Full automatic detection of tree species based on delineated single tree crowns - a data fusion approach for airborne laser scanning data and aerial photographs. In *Silvilaser 2008*. Edinburgh, UK: 76-85.

- Hu, B., Li, J., Jing, L., & Judah, A. (2014). Improving the efficiency and accuracy of individual tree crown delineation from high-density LiDAR data. *International Journal of Applied Earth Observation and Geoinformation*, 26(0), 145-155. doi: <http://dx.doi.org/10.1016/j.jag.2013.06.003>
- Hu, B., & Zhang, K. (2012). Individual urban tree species classification using very high spatial resolution airborne multi-spectral imagery using longitudinal profiles. *Remote Sensing*, 4(12), 1741-1757. doi: 10.3390/rs4061741
- Huete, A. R., & Warrick, A. W. (1990). Assessment of vegetation and soil water regimes in partial canopies with optical remotely sensed data. *Remote Sensing of Environment*, 32(2-3), 155-167. doi: [http://dx.doi.org/10.1016/0034-4257\(90\)90015-E](http://dx.doi.org/10.1016/0034-4257(90)90015-E)
- Hug, C., Krzystek, P., & Fuchs, W. (2004). Advanced LiDAR data processing with LASTools. *GeoLas Consulting*, D-85586. Retrieved on January 2014 from <http://cartesia.org/geodoc/isprs2004/comm2/papers/240.pdf>
- Hung, C., Bryson, M., & Sukkarieh, S. (2012). Multi-class predictive template for tree crown detection. *International Journal of Photogrammetry and Remote Sensing (ISPRS)*, 68, 170-183. doi: DOI 10.1016/j.isprsjprs.2012.01.009
- Hutchinson, C. F. (1982). Techniques for combining Landsat and ancillary data for digital classification improvement. *Photogrammetric Engineering and Remote Sensing*, 48(1), 123-130.
- Hyyppä, J., Hyyppä, H., Litkey, P., Yu, X., Haggrén, H., Rönholm, P., Pyyalo, U., Pitkänen, J., & Maltamo, M. (2004). Algorithms and methods of airborne laser scanning for forest measurements. *International Archive of Photogrammetry, Remote Sensing and Spatial Information Science*, XXXVI(8), 82-89.
- Hyyppä, J., Kelle, O., Lehikoinen, M., & Inkinen, M. (2001). A segmentation-based method to retrieve stem volume estimates from 3-D tree height models produced by laser scanners. *Transactions on Geoscience and Remote Sensing*, 39(5), 969-975. doi: Doi 10.1109/36.921414
- Jackson, R. D., & Huete, A. R. (1991). Interpreting vegetation indices. *Preventive Veterinary Medicine*, 11(3-4), 185-200. doi: [http://dx.doi.org/10.1016/S0167-5877\(05\)80004-2](http://dx.doi.org/10.1016/S0167-5877(05)80004-2)
- Jain, A. K. (1989). *Fundamentals of digital image processing*. Prentice Hall (1st ed.), ISBN-10: 0133361659.
- Jakubowski, M., Li, W., Guo, Q., & Kelly, M. (2013). Delineating individual trees from Lidar data: A comparison of vector- and vaster-based segmentation Approaches. *Remote Sensing*, 5(9), 4163-4186. doi: 10.3390/rs5094163

References

- Jiang, D., Zhuang, D., Huang, Y., & Fu, J. (2011). *Survey of multispectral image fusion techniques in remote sensing applications*. Alcorn State University, USA , ISBN 978-953-307-182-4. DOI: 10.5772/10548
- Jing, L., Hu, B., Noland, T., & Li, J. (2012). An individual tree crown delineation method based on multi-scale segmentation of imagery. *International Journal of Photogrammetry and Remote Sensing (ISPRS)*, 70(0), 88-98. doi: <http://dx.doi.org/10.1016/j.isprsjprs.2012.04.003>
- Jovanovic, D., Govedarica, M., & Djordjevic, I.(2011). Presenting and comparing the object based image analysis and standard image analysis for change detection of forest areas, using low-resolution satellite imagery. *11th International Multidisciplinary Scientific Geoconference* , 2, 329-336. DOI: 10.5593/sgem2011/s08.103
- Kato, A., Moskal, L. M., Schiess, P., Swanson, M. E., Calhoun, D., & Stuetzle, W. (2009). Capturing tree crown formation through implicit surface reconstruction using airborne lidar data. *Remote Sensing of Environment*, 113(6), 1148-1162. doi: DOI 10.1016/j.rse.2009.02.010
- Ke, Y., & Quackenbush, L. J. (2011). A review of methods for automatic individual tree-crown detection and delineation from passive remote sensing. *International Journal of Remote Sensing*, 32(17), 4725-4747. doi: 10.1080/01431161.2010.494184
- Ke, Y., Quackenbush, L. J., & Im, J. (2010). Synergistic use of QuickBird multispectral imagery and LIDAR data for object-based forest species classification. *Remote Sensing of Environment*, 114(6), 1141-1154. doi: 10.1016/j.rse.2010.01.002
- Khosravipour, A., Skidmore, A. K., Isenburg, M., Wang, T., & Hussin, Y. A. (2013). Development of an algorithm to generate a Lidar pit-free canopy height model, *SilviLaser 2013*, 125-128. Beijing, China.
- Kim, D. (1998). Multi-resolutional watershed segmentation with user-guided grouping. *Part of the SPIE Conference on Image Processing*, 3338, 1087-1095. San Diego, California SPIE, ISBN: 0819427837
- Kim, D. A., Lee, W. K., Son, Y., Bae, S. W., Kim, C., & Yoo, S. (2010). Estimation of carbon storage based on individual tree detection in *Pinus densiflora* stands using a fusion of aerial photography and LiDAR data. *Science China-Life Sciences*, 53(9), 1162-1162. doi: DOI 10.1007/s11427-010-4064-7
- King, D. J., Bell, F.W. , & Pitt, D. G. (2002). Automated tree crown detection and delineation in high-resolution digital camera

- imagery of coniferous forest regeneration. *Remote Sensing of Environment*, 82, 322–334.
- Koch, B., Heyder, U., & Weinacker, H. (2006). Detection of individual tree crowns in airborne lidar data. *Photogrammetric Engineering and Remote Sensing*, 72(4), 357–363.
- Koetz, B., Morsdorf, F., Van der Linden, S., Curt, T., & Allgower, B. (2008). Multi-source land cover classification for forest fire management based on imaging spectrometry and LiDAR data. *Forest Ecology and Management*, 256(3), 263–271. doi: DOI 10.1016/j.foreco.2008.04.025
- Kukunda, C. B. (2013). *Synergy of Airborne LiDAR data and VHR Satellite Optical Image for Individual Crown and Tree Species Identification* (Master thesis), Available from Repository ITC publications. Retrieved from http://itc.nl/library/papers_2013/msc/gem/kukunda.pdf
- Leckie, D., Gougeon, F., Hill, D., Quinn, R., Armstrong, L., & Shreenan, R. (2003). Combined high-density lidar and multispectral imagery for individual tree crown analysis. *Canadian Journal of Remote Sensing*, 29(5), 633–649.
- Li, Z., & Eastman, J. R. (2006). The nature and classification of unlabelled neurons in the use of Kohonen's self-organizing map for supervised classification. *Transactions in GIS*, 10(4), 599–613. doi: 10.1111/j.1467-9671.2006.01014.x
- Lillesand, T., Kiefer, R. W., & Chipman, J. (2007). *Remote Sensing and Image Interpretation* (6th ed.). Wiley, ISBN-10: 0470052457.
- Liu, J. G. (2000). Smoothing filter-based intensity modulation: A spectral preserve image fusion technique for improving spatial details. *International Journal of Remote Sensing*, 21(18), 3461–3472. doi: 10.1080/014311600750037499
- Lopez Saez, J., Corona, C., Stoffel, M., Astrade, L., Berger, F., & Malet, J. P. (2011). Dendrogeomorphic reconstruction of past landslide reactivation with seasonal precision: the Bois Noir landslide, southeast French Alps. *Landslides*, 9(2), 189–203. doi: 10.1007/s10346-011-0284-6
- MaCurdy, T. E., & Ryu, K. (2003). Equivalence results in chi-square tests. *Economics Letters*, 80(3), 329–336. doi: [http://dx.doi.org/10.1016/S0165-1765\(03\)00124-1](http://dx.doi.org/10.1016/S0165-1765(03)00124-1)
- Mäkelä, H., & Pekkarinen, A. (2001). Estimation of timber volume at the sample plot level by means of image segmentation and Landsat TM imagery. *Remote Sensing of Environment*, 77(1), 66–75. DOI:10.1016/S0034-4257(01)00194-8
- Maquaire, O., Malet, J. P., Remaitre, A., Locat, J., Klotz, S., & Guillon, J. (2003). Instability conditions of marly hillslopes: towards landsliding or gullying? The case of the Barcelonnette Basin,

References

- South East France. *Engineering Geology*, 70(1-2), 109-130. doi: Doi 10.1016/S0013-7952(03)00086-3
- Maskova, Z., Zemek, F., & Kvet, J. (2008). Normalized difference vegetation index(NDVI) in the management of mountain meadows. *Borwal Environment Research*, 13, 417-432.
- Mather, P. M., Tso, B., & Koch, M. (1998). An evaluation of Landsat TM spectral data and SAR-derived textural information for lithological discrimination in the Red Sea Hills, Sudan. *International Journal of Remote Sensing*, 19(4), 587-604. doi: 10.1080/014311698215874
- Maurer, T. (2013). How to pan-sharpen images using the gram-schmidt pan-sharpen method- a recipe. *International Archives of the Photogrammetry, Remote Sensing and Spatial Information Sciences, Volume XL-1/W1*, 239-244 .
- Mohan, J. R. R., Sadasivuni, S. S., Durbha, D. L., & Evans, L. B. (2009). Biomass and health based forest cover delineation using spectral un-mixing. *American Society for Photogrammetry and Remote Sensing, 2009 Annual Conference*, Baltimore, MD. Retrieved from <http://srs.fs.usda.gov/pubs/33833>
- Novoty, J., Hanus, J., Lukes, P., & Kaplan, V. (2011). Individual tree crowns delineation using local maxima approach and seeded region growing technique. *GIS Ostrava*. Retrieved from <http://hdl.handle.net/11104/0006456>
- Ørka, H. O., Gobakken, T., Næsset, E., Ene, L., & Lien, V. (2012). Simultaneously acquired airborne laser scanning and multispectral imagery for individual tree species identification. *Canadian Journal of Remote Sensing*, 38(02), 125-138. doi: 10.5589/m12-021
- Ozdemir, I., & Karnieli, A. (2011). Predicting forest structural parameters using the image texture derived from WorldView-2 multispectral imagery in a dryland forest, Israel. *International Journal of Applied Earth Observation and Geoinformation*, 13(5), 701-710. doi: <http://dx.doi.org/10.1016/j.jag.2011.05.006>
- Pascual, C., García-Abril, A., García-Montero, L. G., Martín-Fernández, S., & Cohen, W. B. (2008). Object-based semi-automatic approach for forest structure characterization using lidar data in heterogeneous Pinus sylvestris stands. *Forest Ecology and Management*, 255(11), 3677-3685. doi: <http://dx.doi.org/10.1016/j.foreco.2008.02.055>
- Plackett, R. L. (1900). Karl Pearson and the Chi-Squared Test. *International Statistical Review / Revue Internationale de Statistique*, 51(1), 59-72. Retrieved from <http://www.jstor.org/stable/1402731>

- Persson, O. G., Fairall, C. W., Andreas, E. L., Guest, P. S., & Perovich, D. K. (2002). Measurements near the Atmospheric Surface Flux Group tower at SHEBA: Near-surface conditions and surface energy budget. *Journal of Geophysical Research-Space Physics*, 107. doi: doi: 10.1029/2000JC000705
- Pfeifer, N., Mandlbürger, G., Otepka, J., & Karel, W. (2013). OPALS – A framework for Airborne Laser Scanning data analysis. *Computers, Environment and Urban Systems*. ISSN 0198-9715. doi: <http://dx.doi.org/10.1016/j.compenvurbsys.2013.11.002>
- Pinter, P. J., Jackson, R. D., Idso, S. B., & Reginato, R. J. (1983). Diurnal patterns of wheat spectral reflectances. *Geoscience and Remote Sensing, IEEE Transactions on, GE-21(2)*, 156-163. doi: 10.1109/tgrs.1983.350484
- Pinz, A. (1991). A computer vision system for recognition of trees in aerial photographs. In *Proceedings of the International Association of pattern recognition Workshop*, 111-124.
- Pohl, C., & Van Genderen, J. L. (1998). Review article Multisensor image fusion in remote sensing: Concepts, methods and applications. *International Journal of Remote Sensing*, 19(5), 823-854. doi: 10.1080/014311698215748
- Pollock, R. J. (1996). *The automatic recognition of individual trees in aerial images of forests based on a synthetic tree crown image model* (PHD dissertation). Available from: ACM Digital Library. ISBN:0-612-14815-7 . Retrieved from <http://dl.acm.org/dl.cfm?CFID=414786657&CFTOKEN=37729828>
- Pollock, R. J. (1998). Individual tree recognition based on a synthetic tree crown image model. *Paper presented at the Proc. of the International Forum on Automated Interpretation of High Spatial Resolution Digital Imagery for Forestry*. Victoria, BC: Canadian Forest Service, Pacific Forestry Center, pp. 25-34.
- Pouliot, D., King, D., Bell, F., & Pitt, D. (2002). Automated tree crown detection and delineation in high-resolution digital camera imagery of coniferous forest regeneration. *Remote Sensing of Environment*, 82(2), 322-334.
- Razak, K. A., Straatsma, M. W., Van Westen, C. J., Malet, J. P., & de Jong, S. M. (2011). Airborne laser scanning of forested landslides characterization: Terrain model quality and visualization. *Geomorphology*, 126(1-2), 186-200. doi: DOI 10.1016/j.geomorph.2010.11.003
- Reitberger, J., Schnörr, C., Krzystek, P., & Stilla, U. (2009). 3D segmentation of single trees exploiting full waveform LIDAR data. *International Journal of Photogrammetry and Remote*

References

- Sensing (ISPRS)*, 64(6), 561-574. doi:
<http://dx.doi.org/10.1016/j.isprsjprs.2009.04.002>
- Reitberger, J., Krzystek, P., & Heurich, M. (2006). Full-waveform analysis of small footprint airborne laser scanning data in the Bavarian forest national park for tree species classification. *3D Remote Sensing in Forestry*, 218-227. Retrieved from www.researchgate.net/.../236963689_Fullwaveform_analysis..
- Ricchetti, E. (2000). Multispectral satellite image and ancillary data integration for geological classification. *Photogrammetric Engineering and Remote Sensing*, 66(4), 429-435.
- Ruparelia, S. (2012). *Implementation of Watershed Based Image Segmentation Algorithm in FPGA* (Master thesis), Available from University of Stuttgart , Nr.3256. Retrieved from ftp://ftp.informatik.unistuttgart.de/pub/library/medoc.ustuttgart_fi/MSTR-3256/MSTR-3256.pdf
- Skidmore, A. K. (1989). An expert system classifies Eucalypt forest types using thematic mapper data and a digital terrain model. *Photogrammetric Engineering and Remote Sensing*, 55(10), 1449-1464.
- Song, C., Dickinson, M. B., Su, L., Zhang, S., & Yaussey, D. (2010). Estimating average tree crown size using spatial information from Ikonos and QuickBird images: Across-sensor and across-site comparisons. *Remote Sensing of Environment*, 114(5), 1099-1107. doi: doi: 10.1016/j.rse.2009.12.022
- Strahler, A. H., Woodcock, C. E., & Smith, J. A. (1986). On the nature of models in remote-sensing. *Remote Sensing of Environment*, 20(2), 121-139. doi: doi: 10.1016/0034-4257(86)90018-0
- Suarez, J. C., Ontiveros, C., Smith, S., & Snape, S. (2005). Use of airborne LiDAR and aerial photography in the estimation of individual tree heights in forestry. *Computers & Geosciences*, 31(2), 253-262. doi: DOI 10.1016/j.cageo.2004.09.015
- Swatantran, A., Dubayah, R., Roberts, D., Hofton, M., & Blair, J. B. (2011). Mapping biomass and stress in the Sierra Nevada using lidar and hyperspectral data fusion. *Remote Sensing of Environment*, 115(11), 2917-2930. doi: 10.1016/j.rse.2010.08.027
- Tiruveedhula, M., Fan, J., Sadasivuni, R. R., Durbha, S. S., & Evans, D. L. (2009). Biomass and health based forest cover delineation using spectral un-mixing. *American Society for Photogrammetry and Remote Sensing 2009 Annual Conference*, Baltimore, MD. Retrieved from <http://www.srs.fs.usda.gov/pubs/33833#sthash.Q4KMIj7j.dpf>
- Vastaranta, M., Kankare, V., Holopainen, M., Yu, X. W., Hyyppa, J., & Hyyppa, H. (2012). Combination of individual tree detection and area-based approach in imputation of forest variables

- using airborne laser data. *International Journal of Photogrammetry and Remote Sensing (ISPRS)*, 67, 73-79. doi: DOI 10.1016/j.isprsjprs.2011.10.006
- Wang, L., Gong, P., & Biging, G. S. (2004). Individual tree-crown delineation and treetop detection in high-spatial-resolution aerial imagery. *Photogrammetric Engineering & Remote Sensing*, 70(3), 351-357.
- Wang, F. G., & Xu, Y. J. (2010). Comparison of remote sensing change detection techniques for assessing hurricane damage to forests. *Environmental Monitoring and Assessment*, 162(1-4), 311-326. doi: 10.1007/s10661-009-0798-8
- Wang, H., & Dong, Y. (2007). An improved image segmentation algorithm based on Otsu method. *International Symposium on Photoelectronic Detection and Imaging 2007: Related Technologies and Applications*. Edited by Zhou, Liwei. *Proceedings of the SPIE, Volume 6625*. doi: DOI: 10.1117/12.790781
- Willers, J. L., Milliken, G. A., Jenkins, J. N., O'Hara, C. G., Gerard, P. D., Reynolds, D. B., . . . Hood, K. B. (2008). Defining the experimental unit for the design and analysis of site-specific experiments in commercial cotton fields. *Agricultural Systems*, 96(1-3), 237-249. doi: DOI 10.1016/j.agsy.2007.09.003
- Willers, J. L., Wu, J., O'Hara, C., & Jenkins, J. N. (2012). A categorical, improper probability method for combining NDVI and LiDAR elevation information for potential cotton precision agricultural applications. *Computers and Electronics in Agriculture*, 82(0), 15-22. doi: <http://dx.doi.org/10.1016/j.compag.2011.11.010>
- Wulder, M. & Franklin, S. E. (2003). *Remote Sensing of Forest Environments: Concepts and Case Studies*, 135-150. Kluwer Academic publisher, Springer. ISBN-10: 1402074050
- Wulder, M., Niemann, O. K., & Goodenough, D. G. (2000). Local maximum filtering for the extraction of tree locations and basal area from high spatial resolution imagery. *Remote Sensing of Environment*, 73(1), 103-114.
- Zhang, J., & Hu, J. (2008). Image segmentation based on 2D Otsu method with histogram analysis. *International Conference on Computer Science and Software Engineering*, 105-108. doi: 10.1109/csse.2008.206

Appendices

Appendix 1: Marker-Controlled Watershed segmentation algorithm codes in Matlab

```
%% MARKER-CONTROLLED WATERSHED SEGMENTATION ALGORITHM
CANOPY HEIGHT MODEL (LIDAR) INPUT
% Major plan to run the watershed segmentation for crown
delineation.
% How to separate touching objects in an image.
% Definition of algorithm: The watershed transform finds
"catchment basins"
% and "watershed ridge lines" in an image by treating it as
a surface where
% light pixels are high and dark pixels are low.
% Segmentation using the watershed transform works better
if you can
% identify, or "mark," foreground objects and background
locations.
% Basic procedure:
% 1) Compute a segmentation function
% 2) Compute foreground markers, connected blobs of pixels,
linked pixels
% 3) Compute background markers, pixels not belong to any
object
% 4) Modify segmentation function
% 5) Compute the watershed transform

clc
clear all

% Define the function for the watershed algorithm.
% Read the multispectral, NDVI and CHM images separately
specially multispectral and then convert it to a Greyscale.
% Multispectral data import and read should done separately
and then convert it to a Greyscale in another m-file and
then combine with NDVI image by matching the type of data.
Instead of %imread %imscale can also be used.

CIR = multibandread('low.tif', [256, 256, 1],
'uint16=>uint16', 128, 'bil', 'ieee-le',
{'Band','Direct',[4 3 2]});
figure, imshow(CIR),title('MultiSpectral GeoEye-2, low
density subset')
% read all gray scale images separately.
I1 = decorrstretch(CIR, 'Tol',0.1);
I2 = imread('chm_low2.tif');
```

```

figure, imshow(I2), title('Canopy hieght model, low density
subset')
I3 = imread('ndvi_low.tif');

% Fuse or combine the images two by two, add function could
also be used here, both inputs should be in same size and
characteristic of gray scale. Method for combine could also
define, check MATLAB help, image processing toolbox.
I = imfuse(I2,I1,I3);
I = imadd (I2,I1,I3);

figure, imshow(I), title('low density subset')

% Gradient Magnitude as the Segmentation Function, for
detect edges.
% The gradient is high at the borders of the objects and
low (mostly)
% inside the objects.
hy = fspecial('sobel');
% Sobel is edge detector filter
hx = hy;
Iy = imfilter(double(I), hy, 'replicate');
Ix = imfilter(double(I), hx, 'replicate');
gradmag = sqrt(Ix.^2 + Iy.^2);
figure, imshow(gradmag,[]), title('Gradient magnitude,
Barcelonatte')
figure, hist(gradmag), title('Low density subset area
histogram')
% 3D visualization
figure, mesh(gradmag), title('Low density subset area mesh
graph')

% Without additional preprocessing such as the marker
computations below,
% using the watershed transform directly often results in
% "oversegmentation."

% Mark the foreground markers, morphological techniques.
% Opening is an erosion followed by a dilation, based on
shape & parameter.
SE = strel ('disk', 1);
% Disk creates a flat, disk-shaped structuring element,
% where R specifies the radius.
IO = imopen(I, SE);
figure, imshow(IO), title('Opening (low density subset)')

% Compute the opening-by-reconstruction
IE = imerode(I, SE);

```

References

```
IOBR = imreconstruct(IE, I);
% Uses 8-connected neighborhoods for 2-D images.
figure, imshow(IOBR), title('Opening-by-reconstruction (low
density subset)')

% Following closing can remove the dark spots and stem
marks.
% Close based on Opening.
IOC = imclose(IO, SE);
figure, imshow(IOC), title('Opening-closing (low density)')

% Close based on open imreconstruct.
IOBRD = imdilate(IOBR, SE);
IOBRDCBR = imreconstruct(imcomplement(IOBRD),
imcomplement(IOBR));
IOBRDCBR = imcomplement(IOBRDCBR);
figure, imshow(IOBRDCBR), title('Opening-closing by
reconstruction (low density subset)')

% Reconstruction-based opening and closing are more
effective than standard
% opening and closing at removing small blemishes without
affecting the
% overall shapes of the objects.

% Calculation of regional maxima to obtain good foreground
markers.
FGM = imregionalmax(IOBRDCBR, 4);
figure, imshow(FGM), title('Regional maxima of opening-
closing by reconstruction (low density subset)')

% Superimpose the foreground marker image on the original
image.
I2 = I;
I2(FGM) = 255;
figure, imshow(I2), title('Regional maxima superimposed on
original image (low density subset)')

% Smooth the results & the image
% For properly segmentation clean the edges of the marker
blobs and
% then shrink them a bit.
% Returns an array the same size
SE2 = strel(ones(2,2));
FGM2 = imclose(FGM, SE2);
FGM3 = imerode(FGM2, SE2);
% Erodes the grayscale, binary, or packed binary image IM,
returning
```

```
% the eroded image IM2
FGM4 = bwareaopen(FGM3, 1);
% Removes from a binary image all connected components
(objects) that
% have fewer than P pixels, producing another binary image.
I3 = I;
I3(FGM4) = 255;
figure, imshow(I3)
title('Modified regional maxima superimposed on original
image (low density subset)')

% Compute Background Markers
BW = im2bw(IOBRCEBR, graythresh(IOBRCEBR));
% Convert image to binary image, based on threshold.
% Global image threshold using Otsu's method, a normalized
intensity
% value that lies in the range [0, 1].
figure, imshow(BW), title('Thresholded opening-closing by
reconstruction (low density subset)')
D = bwdist(BW);
DL = watershed(D);
bgm = DL == 0;
figure, imshow(bgm), title('Watershed ridge lines (low
density subset)')

% Compute the Watershed Transform of the Segmentation
Function.
% The function imimposemin can be used to modify an image
so that it has
% regional minima only in certain desired locations.
gradmag2 = imimposemin(gradmag, bgm | FGM4);

% Compute the watershed-based segmentation.
% Computes a label matrix identifying the watershed
regions.
L = watershed(gradmag2);

% Visualize the Result.
% Visualization technique is to superimpose the foreground
markers,
% background markers, and segmented object boundaries on
the original image.
I4 = I;
% Dilate image
I4(imdilate(L == 0, ones(2,2)) | bgm | FGM4) = 255;
% L is counter of belonging to a specific region, 0 means
to do not belong,
```

References

```
% The elements labeled 1 belong to the first watershed
region, then
% labeled 2 belong to the second watershed region, and so
on.
figure, imshow(I4)
title('Markers and object boundaries superimposed on
original image (low density subset)')
% Visualization illustrates how the locations of the
foreground and
% background markers affect the result.

% Visualization of Index of segmentation figure;
imagesc(L); colormap(rand(1000,3)); axis image
% Export boundary of segments based on their index
Lboundary = (L==0);
% Visualization of boundry index
figure; imagesc(Lboundary); colormap(gray(2)); axis image
% Save the result with coordinates and projection system in
TIF format
imwrite(L, 'segmentedCHM.tif', 'tiff')
imwrite(Lboundary, 'segmentBoundariesCHM.tif', 'tiff')
```